PREPARATION AND CHARACTERIZATION OF HIGH-PERFORMANCE POLY(LACTIC ACID) NANOCOMPOSITES FOR BIOMEDICAL APPLICATIONS

by

Artur Daniel Moreira Pinto

Dissertation presented in Advanced Institute of Health Sciences – North for the degree of

Master in Molecular Therapies

November 2011

Project Developed

at

Faculty of Engineering of University of Porto

LEPAE – Laboratory for Process, Environmental and Energy Engineering

Supervisor

Professor Dr. Fernão D. Magalhães

November 2010 - November de 2011

AGRADECIMENTOS

Em primeiro lugar, quero agradecer à minha família por todo o amor que têm por mim e pela educação que me deram; vocês são o alicerce de tudo o que alguma vez possa construir.

Depois, dizer que desde o primeiro dia até à conclusão do presente trabalho, sempre tive todo o apoio e recursos de que precisei. Sem a inesgotável disponibilidade do meu orientador, esta tese não existiria. Obrigado professor Fernão, é um orientador e uma pessoa excepcional.

Quero ainda agradecer a todas as pessoas do LEPAE, FEUP e ARCP que me ajudaram neste período, como por exemplo: o Alfredo, o Pedro e o Rui com quem muito aprendi e discuti sobre a química do grafeno; o professor Adélio e a Joana Cabral pela paciência e colaboração no combate contra as fugas; todos os colegas de laboratório pelos pequenos grandes favores do dia-a-dia de trabalho; a Sarah Pontes e a Eva Ribeiro pela ajuda na gestão do projecto e simplificação dos processos burocráticos.

Não posso esquecer a Susana, o professor Miguel Gama e a Paula, da Universidade do Minho, a quem agradeço pela colaboração na realização dos ensaios biológicos. Estes ensaios foram extremamente importantes para a tese, agradeço mais uma vez à incansável Susana pelos largos meses de trabalho.

Termino agradecendo a todas as pessoas que durante o meu percurso académico contribuíram para a minha formação; como: a professora Odília Queirós e a professora Roxana Moreira, do mestrado em Terapias moleculares, que sempre me incentivaram, apoiaram, com quem muito aprendi e que me deram a oportunidade de investigar e dar aulas, o que em parte motivou a minha opção de tentar seguir a carreira académica; o professor Bruno Sarmento, que me orientou desde o final da licenciatura e me mostrou o caminho a seguir para ser investigador; a professora Elsa Cardoso, com quem nos primeiros anos de licenciatura participei num projecto de investigação CESPU alunos, dando assim os primeiros passos extra-aulas num laboratório.

TABLE OF CONTENTS

ABSTRACT

Poly(lactic acid) (PLA) has several applications in biomedicine (sutures, scaffolds, implants, drug micro/nanoencapsulation). This aliphatic polyester is prepared from lactic acid (therefore derived from 100 % renewable sources, *e.g.* corn or sugarcane), biodegradable, biocompatible and has a low cost. [1][2] In order to make this material more attractive to the mentioned applications, as a valid alternative to petrochemical plastics, some properties should be improved, namely mechanical resistance and gas permeability. [3]

Graphene, the elementary structure of graphite, is an atomically thick sheet composed of sp^2 carbon atoms arranged in a flat honeycomb structure, possesses remarkable mechanical strength (Young's modulus = 1 TPa, tensile strength = 130 GPa), an extremely high surface area (theoretical limit: 2630 $m^2 \cdot g^{-1}$) and is impermeable to gases. Graphene oxide (GO) is similar to graphene, but presents several oxygen-containing functional groups (*e.g.* hydroxyls, epoxides, and carbonyls). The presence of these polar groups reduces the thermal stability of the nanomaterial, but may be important to promote interaction and compatibility with a particular polymer matrix. [4] [5] It has been shown in studies with mice that GO is biocompatible [6] up to blood concentrations of 10 $mg \cdot kg^{-1}$ [7]; since only small amounts of graphene oxide are needed to reinforce poly(lactic acid), these nanocomposites could be used in food/medicines protection materials [3] and biomedical technology. [8]

Effective mechanical reinforcement of polymeric materials using very small wt. % of GO has been reported by several authors. Wang and co-workers, improved the Young´s modulus of chitosan by 51% and the tensile strength by 91% incorporating 1 wt. % GO [9]. An increase of about 75% in polypropylene's Young´s modulus and yield strength was achieved at 0.42 wt. % GO loading by Song and co-workers. [10] Cao and co-workers increased Young´s modulus of PLA by 18 % with only 0.2 wt. % of reduced GO. [11]

Graphene oxide and graphene had been reported as efficient drug carriers [12] [13]. PLA is also used for this purpose [14]; development of hybrid vehicles for drug targeting can take advantage of both materials properties and originate synergistic effects. [15] Also several graphene based biosensors are being developed [16], these sensors can be used, for example, to detect drug concentrations on target places. Recent studies show that graphene substractes promote adherence of human mesenchymal

stromal cells and osteoblasts [17], which can lead to better performance on tissues recovery using scaffolds containing graphene and graphene oxide. Due to their great potential several approaches are under study for future applications of these nanomaterials in biomedical engineering and biotechnology. [18]

In this work, nanocomposite poly(lactic acid) (PLA) thin films were produced incorporating small amounts (0.2 to 1 wt. %) of graphene oxide (GO) and graphene nanoplatelets (GNP). Films were prepared by solvent-casting. Mechanical properties were evaluated for plasticized (by residual solvent) and unplasticized films. Plasticized nanocomposite films presented yield strength and Young´s modulus about 100 % higher than pristine PLA. For unplasticized films improvements in tensile strength and Young´s modulus were about 15 % and 85 %, respectively. For both film conditions, a maximum in mechanical performance was identified for about 0.4 wt. % loadings of the two filler materials tested. Permeabilities towards O_2 and N_2 decreased respectively three and fourfold in films loaded with both GO or GNP. The glass transition temperature showed maximum increases, in relation to unloaded PLA films, of 5 ºC for 0.4 % GO, and 7 ºC for 0.4 % GNP, coinciding with the observed maximums in mechanical properties. The incorporation of GO and GNP on PLA at low loadings (0.4 wt. %), don´t affect cellular proliferation at the surface of the resultant nanocomposites. This allows GNP and GO dispersion on polymers in order to obtain high performance materials for biomedical applications.

Future work will be focused on improving the synthesized materials mechanical and gas barrier performance by optimizing the surface oxidation level and using different manufacture processes. Other biological assays will be performed to assure composite biocompatibility and to characterize it´s “in vitro” and “in vivo” behavior.

CHAPTER 1

INTRODUCTION

1.1 Biomaterials and Biocompatibility

Biomaterials are materials of natural or man-made origin that are used to direct, supplement, or replace the functions of living tissues of the human body. When in the form of implants (sutures, bone plates, joint replacements, ligaments, vascular grafts, heart valves, intraocular lenses, dental implants, etc.) and medical devices (pacemakers, biosensors, artificial hearts, blood tubes, etc.) are widely used to replace and/or restore the function of traumatized or degenerated tissue or organs, to assist in healing, to improve function and to correct abnormalities.

Biocompatibility comprises surface and structural compatibility. The first concerns chemical, biological, and physical suitability and the second imply optimal adaptation to the mechanical behavior of the host tissues. Therefore, structural compatibility refers to the mechanical properties of the implant material, implant design, and optimal load transmission at the implant/tissue interface. Despite of biomaterial characteristics, it success in the body also depends of other factors such as surgical technique, health condition and activities of the patient. Most materials used in biomedical applications are metals, ceramics or polymers. These materials can be classified as bioinert and bioactive, biostable and biodegradable, etc. [19]

1.2 Polymers

Polymers are large molecules synthesized from smaller molecules, called monomers. Most polymers are organic compounds with carbon as the base element. They are frequently classified by their synthesis mechanism: step growth or chain addition. In step growth polymerization stepwise reactions occur between end functional groups. Linear polymers are formed when each monomer has two functional groups (functionality = 2). If at least one of the monomers has higher functionality, branched polymers will be formed. The second type of polymerization is chain polymerization where monomers are added one at a time to the growing polymer chain. Properties of

the polymers can be predicted and explained by understanding the polymer structure on the atomic, microscopic, and macroscopic scale.

Polymers can be roughly classified into two main classes, thermoplastic and thermoset. Thermoplastic polymers are made of individual polymer chains, held together by relatively weak van der Waals and dipole-dipole forces, which can be linear or branched. Thermosetting polymers contain cross-links between polymer chains. Cross-links are covalent bonds between chains and can be formed using monomers with functionalities greater than two during synthesis. Unlike thermoplastics, thermoset polymers cannot be melted or reprocessed.

Polymers in the solid state have varying degrees of crystallinity. No polymer is truly 100 percent crystalline, but some are purely amorphous. Polymer chains folding over themselves form crystalline regions. Amorphous polymer regions connect these crystalline regions. Polymer chains are packed tighter in crystalline regions leading to higher intermolecular forces. This means that mechanical properties such as modulus and strength increase with crystallinity. Ductility decreases with crystallinity since polymer chains have less room to slide past each other. The primary requirement for crystallinity is an ordered repeating chain structure. This is why stereoregular polymers are often crystalline and their irregular counterparts are amorphous. Stereoregular polymers have an ordered stereostructure: either isotactic or syndiotactic. Isotactic polymers have the same configuration at each stereo center, while configuration alternates for syndiotactic polymers. Atactic polymers have no pattern to their stereostructure.

Some polymers are stiff, hard plastics at room temperature, while others are soft and flexible at room temperature. The temperature at which hard to soft transformation takes place is called the glass transition temperature (*Tg*). Differential thermal analysis (DTA) or a similar technique called differential scanning calorimetry (DSC) can be used to determine the temperature at which phase transitions such as glass transition temperature and melting temperature *Tm* occur. DSC involves heating a polymer sample along with a standard that has no phase transitions in the temperature range of interest. The ambient temperature is increased at a regular rate and the difference in temperature between the polymer and the standard measured. The glass transition is endothermic; therefore, the polymer sample will be cooler compared to the standard at *Tg*. Similarly, melting is endothermic and will be detected as a negative temperature compared to the standard. If the polymer was quenched from melt prior to DSC

analysis, it may be amorphous even though it has the potential to crystallize. In this case, the sample will crystallize during the DSC run at a temperature between the *Tg* and *Tm*. A polymer that does not crystallize would show a glass transition only and the crystallization and melting peaks would be absent. These measurements can be made to identify an unknown plastic, or to aid in the synthesis of new polymers with desired changes in mechanical properties at certain temperatures. [20]

Biodegradable polymeric biomaterials could be generally divided into eight groups based on their chemical origin:

1. biodegradable linear aliphatic polyesters (e.g., polyglycolide, polylactide, polycaprolactone, polyhydroxybutyrate) and their copolymers within the aliphatic polyester family like poly(glycolide-L-lactide) copolymer and poly(glycolide- ε -caprolactone) copolymer;
2. biodegradable copolymers between linear aliphatic polyesters in 1) and monomers other than linear aliphatic polyesters like, poly(glycolide-trimethylene carbonate) copolymer, poly(L-lactic acid-L-lysine) copolymer, Tyrosinebased polyarylates or polyiminocarbonates or polycarbonates, poly(D,L-lactide-urethane), and poly(esteramide);
3. polyanhydrides;
4. poly(orthoesters);
5. poly(ester-ethers) like poly-p-dioxanone;
6. biodegradable polysaccharides like hyaluronic acid, chitin and chitosan;
7. polyamino acids like poly- L-glutamicacid and poly-L-lysine;
8. inorganic biodegradable polymers like polyphosphazene and poly[bis(carboxylatophenoxy)phosphazene] which have a nitrogen-phosphorus backbone instead of ester linkage. [21]

Biodegradable biomaterials should generate non-toxic degradation products, susceptible to metabolization and clearance. Depending on the mode of degradation, polymeric biomaterials can be further classified into hydrolytically degradable polymers and enzymatically degradable polymers. Most of the naturally occurring polymers undergo enzymatic degradation. Natural polymers possess several inherent advantages such as bioactivity, the ability to present receptor-binding ligands to cells, susceptibility to cell-

triggered proteolytic degradation and natural remodeling. The inherent bioactivity of these natural polymers has its own downsides. These include a strong immunogenic response associated with most of the polymers, the complexities associated with their purification and the possibility of disease transmission.

Synthetic biomaterials on the other hand are generally biologically inert, they have more predictable properties and batch-to-batch uniformity and they have the unique advantage having tailored property profiles for specific applications, devoid of many of the disadvantages of natural polymers. Hydrolytically degradable polymers are generally preferred as implants due to their minimal site-to-site and patient-to-patient variations compared to enzymatically degradable polymers. Extensive research has gone since then to custom designing biodegradable polymer systems with predictable erosion kinetics as drug/gene delivery vehicles, scaffolds for tissue engineering, suture systems or as transient implants for orthopedic and related medical applications. [19]

The earliest, most successful and frequent biomedical applications of biodegradable polymeric biomaterials have been in wound closure. All biodegradable wound closure biomaterials are based upon the glycolide and lactide families. For example, polyglycolide (Dexon from American Cyanamid), poly(glycolide-L-lactide) random copolymer with 90 to 10 molar ratio (Vicryl from Ethicon), poly(ester-ether) (PDS from Ethicon), poly(glycolide-trimethylene carbonate) random block copolymer (Maxon from American Cyanamid), and poly(glycolide- ε -caprolactone) copolymer (Monocryl from Ethicon). This class of biodegradable polymeric biomaterials is also the one most studied for their chemical, physical, mechanical, morphological, and biological properties and their changes with degradation time and environment. Some of the above materials like Vicryl have been commercially used as surgical meshes for repair of a hernia or the body wall. The next largest biomedical application of biodegradable polymeric biomaterials that are commercially satisfactory is drug control/release devices. Some well-known examples in this application are polyanhydrides and poly(ortho-ester). Biodegradable polymeric biomaterials, particularly totally resorbable composites, have also been experimentally used in the field of orthopedics, mainly as components for internal bone fracture fixation like PDS pins. However, their wide acceptance in other parts of orthopedic implants may be limited due to their inherent mechanical properties and their biodegradation rate. Besides the commercial uses described above, biodegradable polymeric biomaterials have been experimented with as: vascular grafts, vascular stents, vascular couplers for vessel anastomosis, nerve

growth conduits, augmentation of defected bone, ligament/tendon prostheses, intramedullary plug during total hip replacement, anastomosis ring for intestinal surgery, and stents in ureteroureterostomies for accurate suture placement. [21]

Ring opening polymerization is an extensively investigated route to develop hydrolytically sensitive polymers, including the poly(α-esters) and polyphosphazenes. Poly(α-esters) are thermoplastic polymers with hydrolytically labile aliphatic ester linkages in their backbone. Although all polyesters are theoretically degradable as esterification is a chemically reversible process, only aliphatic polyesters with reasonably short aliphatic chains between ester bonds can degrade over the time frame required for most of the biomedical applications. Poly(α-esters) comprise the earliest and most extensively investigated class of biodegradable polymers. The uniqueness of this class of polymers lies in its immense diversity and synthetic versatility. Poly(a-ester)s can be developed from a variety of monomers via ring opening and condensation polymerization routes depending on the monomeric units. Bacterial bioprocess routes can also be used to develop some poly(α-ester)s. Among the class of poly(a-ester)s, the most extensively investigated polymers are the poly(ahydroxy acid)s, which include poly(glycolic acid) and the stereoisomeric forms of poly(lactic acid). Lactide is a chiral molecule and exist in two optically active forms: L-lactide and D-lactide. The polymerization of these monomers leads to the formation of semi-crystalline polymers. The polymerization of racemic (D,L)-lactide and mesolactide however, results in the formation of amorphous polymers. Among these monomers, L-lactide is the naturally occurring isomer. Similar to polyglycolide, poly(L-lactide) (PLLA) is also a crystalline polymer (aprox. 37% crystallinity) and the degree of crystallinity depends on the molecular weight and polymer processing parameters. It has a glass transition temperature of 60–65 ºC and a melting temperature of approximately 175 ºC. Poly(L-lactide) is a slow-degrading polymer compared to polyglycolide, has good tensile strength, low extension and a high modulus (approximately 4.8 GPa) and hence, has been considered an ideal biomaterial for load bearing applications, such as orthopaedic fixation devices. Some of the PLLA-based orthopaedic products include: the Phantom Soft Thread Soft Tissue Fixation Screws, Phantom Suture Anchors (DePuy), Full Thread Bio Interference Screws (Arthrex), BioScrews, Bio-Anchors, Meniscal Stingers (Linvatec), and the Clearfix Meniscal Darts (Innovasive Devices). PLLA can also form high strength fibers and was FDA approved in 1971 for the development of an

improved suture over DEXONs. Due to the high strength of PLLA fibers, it has been investigated as scaffolding material for developing ligament replacement or augmentation devices to replace nondegradable fibers, such as Dacron. Some PLLA fiber-based devices are currently under investigation as long-term blood vessel conduits. An injectable form of PLLA (Sculptras) has recently been approved by the FDA for the restoration or correction of facial fat loss or lipoatrophy in people with the human immunodeficiency virus. Polylactides undergo hydrolytic degradation via the bulk erosion mechanism by the random scission of the ester backbone. It degrades into lactic acid a normal human metabolic by-product, which is broken down into water and carbon dioxide via the citric acid cycle. [22]

1.3 PLA processing

Today, the main transformation methods for PLA are based on melt processing. This approach involves heating the polymer above its melting point, shaping it to the desired forms, and cooling to stabilize its dimensions.

Prior to melting processing of PLA, the polymer must be dried sufficiently to prevent excessive hydrolysis (causing chain scission and thus molecular weight drop) which can compromise the physical properties of the polymer. Typically the polymer is dried to less than 100 ppm (0.01%, w/w). Drying of PLA takes place in the temperature range of 80–100◦C. The required drying time is dependent on the drying temperature.

Extrusion is the most important technique for continuously melt processing of PLA. The plasticizing extruder can be part of the forming machine systems for injection molding, blow molding, film blowing and melt spinning. Figure 1 shows a schematic representation of the major components of an extruder for an injection molding machine. A typical screw consists of three sections: (1) feed section – acts as an auger which receives the polymer pellets and conveys the polymer into the screw; (2) transition section (also known as compression or melting sections) flight depth decreases gradually, which compresses the pel lets to enhance the friction and contact with the barrel. In order to segregate the molten polymer pool from the pellet unmelted pellets, various barrier flight designs have been adopted; (3) metering section characterized by a constant and shallow flight depth, which acts as a pump to meter accurately the required quantity of molten polymer. The l/d ratio, which is the ratio of flight length of the screw to its outer diameter, determines the shear and residence time

of the melt. Screws with large l/d ratio provide greater shear heating, better mixing, and longer melt residence time in the extruder. Commercial grade PLA resins can typically be processed using a conventional extruder equipped with a general purpose screw of l/d ratio of 24–30.

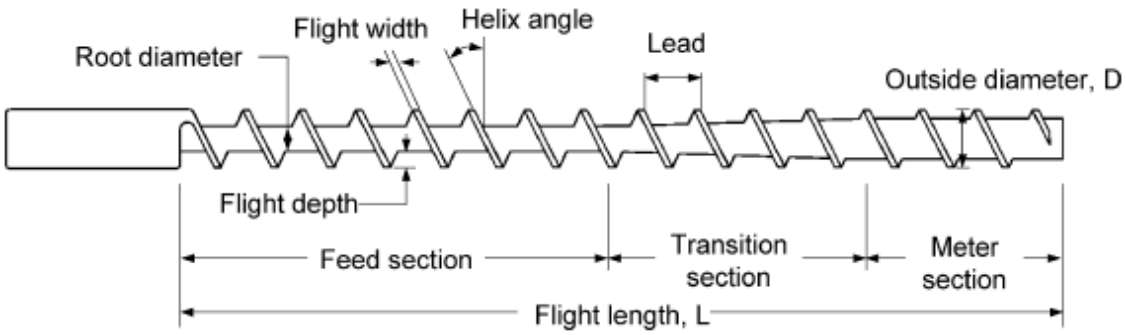

Figure 1 - Typical geometries of a screw for single-screw extruder. [23]

Injection molding is the most widely used converting process for thermoplastic articles, especially for those that are complex in shape and require high dimensional precision. All injection molding machines have an extruder for plasticizing the polymer melt.

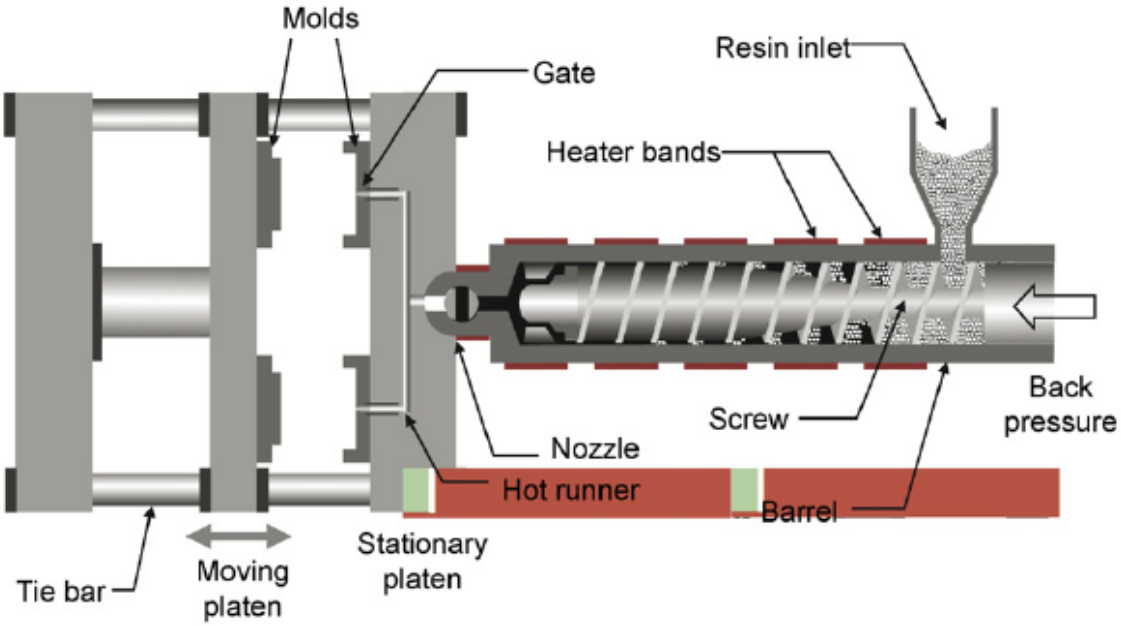

Figure 2 - Major components of an injection molding machine. [23]

A typical cycle for an injection molding machine is presented in figure 2. The beginning of mold close is usually taken as the start of an injection molding cycle. Immediately after the molds clamp up, the nozzle opens and the screw moves forward, injecting the polymer melt into the mold cavity. To compensate for the material shrinkage during cooling in the mold, the screw is maintained in the forward position by a holding pressure. At the end of the holding phase, the nozzle is shut off and the screw begins to recover, while the part continues to be cooled in the mold.

PLA with l-lactide contents of 92–98% have been successfully extruded using conventional extruders. The production of PLA film and sheet is practically identical; the main difference between them is their stiffness and flexibility due to the difference in their thicknesses. Typically, films are ≤0.076mm in thickness, while sheets are typically ≥ 0.25mm. In cast film extrusion, the molten PLA is extruded through a sheet die and quenched on polished chrome rollers that are cooled with circulating water.

In extrusion blow film process, molten PLA is extruded to form a tube using an annular die. By blowing air through the die head, the tube is inflated into a thin tubular bubble and cooled. The tube is then flattened in the nip rolls and taken up by the winder. By varying the, the ratio of bubble diameter to the die diameter, screw speed, air pressure, and winder speed, films of different thicknesses (~10–150 μm) and degree of orientation can be achieved.

Thermoforming is commonly used for forming packaging containers that do not have complicated features. PLA polymers have been successfully thermoformed into disposable cups, single-use food trays, lids, and blister packaging. In this process, PLA sheet is heated to soften the polymer, forced either pneumatic and/or mechanically against the mold, allowed to cool, removed from the mold, and then trimmed. Heating of PLA sheet for thermoforming is generally achieved by infrared red (IR) radiation from heater elements. Each polymer has an optimum IR absorbance frequency in the IR region. Therefore, the heater element should be set at the temperature at which the majority of energy is absorbed by the polymer.

Due to their biocompatibility and large surface area, PLA foams have a niche in tissue engineering and medical implant applications. Foaming of PLA is generally carried out by dissolving a blowing agent in the PLA matrix. The solubility of the blowing agent is then reduced rapidly by producing thermodynamic instability in the structure (e.g., temperature increase or pressure decrease), to induce nucleation of the bubbles. To

stabilize the bubbles, the foam cells are vitrified when the temperature is reduced below the *Tg* of the polymer.

High water vapor transmission rate of PLA often precludes its use in applications where moisture barrier is critical. However, this property can be leveraged for fabricating fibers used in garments (e.g., shirts, dresses, underwear, shoes, etc.) to improve their "breathability". While PLA fibers are not as wettable as cotton, they exhibit much greater water vapor transmission than polyester or nylon fibers. In a two-stage melt spinning process, the polymer is first heated above its melting point and extruded through the spinneret. The solidification of the extrudate is achieved by cooling in the air and the take up roller. In the second stage, the fiber undergoes hot drawing, where the filament is pulled down by a take-up roll with a specific speed to achieve fiber orientation, which is important to increase the tenacity and stiffness of the fibers. PLAcan be melt spun in a high-speed spinning process with take-up velocity of up to 5000 m/min.

Electrospinning is a technique for producing fibers that are much smaller in diameter than those produced using the conventional techniques. Electrospun fibers typically have diameters range from micrometer to nanometer. Electrospinning requires the solubilization of the polymer in a solvent, using electrostatic force to spin the solution into fibers. A typical laboratory electrospinner is made up of four main components: (1) a high voltage DC supply; (2) a spinneret, charged by a DC power supply; (3) an infusion or peristaltic pump to deliver polymer solution to the spinneret; and (4) a metal fiber collector which also acts as a counter electrode (Figure 3). To increase throughput, multiple spinnerets have been used in conjunction with a conveyor belt to achieve a continuous process. Most of the setups reported in the literature involve applying a positive electrode to the spinneret and grounding the counter electrode, although it is also possible to spin fiber by reversing the polarity. The basis of electrospinning is to charge the polymer solution in the spinneret tip with a high voltage such that the induced charges cause the polymer solution to eject and travel towards the ground (or oppositely charged) collector. When the polymer solution is charged, the induced electrostatic repulsion works against the surface tension of the solution, causing the polymer solution to elongate and form a characteristic feature known as a Taylor cone (Figure 3). When the voltage reaches a critical level (typically in the order of 10–20 kV), the electrostatic repulsion overcomes the surface tension of the solution, causing the polymer to eject towards the collector. As the polymer jet takes flight in the air, the

solvent vaporizes rapidly, producing a continuous fiber which deposits on the collector. By allowing the fiber to spin for some time, a nonwoven fibrous mat is formed on the collector.

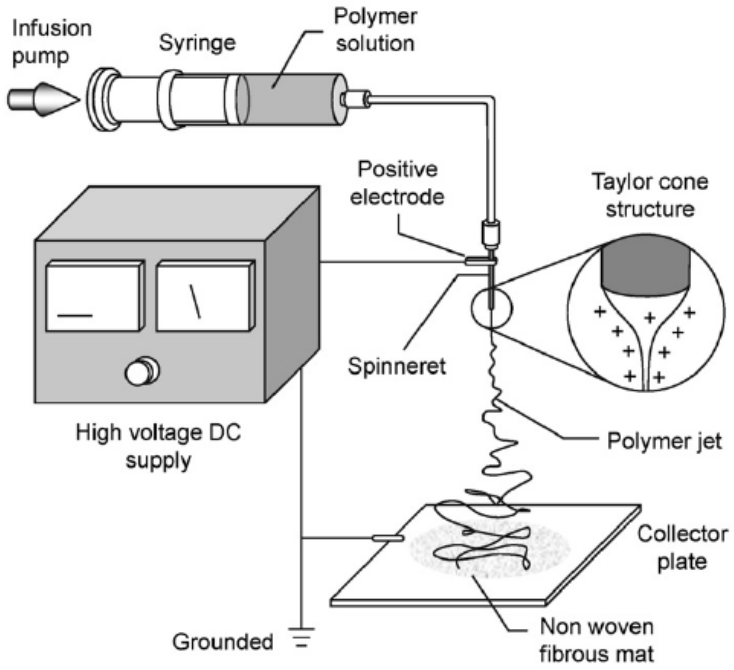

Figure 3 - Typical setup for electrospinning. [23]

Due to their small diameter, electrospun fibers possess very large area, making them an ideal material for applications such as medical tissue scaffold, wound dressing, carrier for drugs, protective fabrics, high performance filter media, filler for nanocomposite materials, etc. PLA has been successfully electrospun into fibers, primarily for tissue engineering and biomedical applications. For instance, a number of studies showed that scaffolds for the regeneration of cardiac, neural, bone and blood vessel tissues can be fabricated from electrospun PLA fiber through post-spinning orientation and/or using rotating target collectors. PLA has been electrospun into different forms of ultrafine fiber and used as carriers for bioactive agents, including antibiotics, anticancer drugs, and antibacterial silver nanoparticles. Other composite PLA fibers containing nano-components such as nanoclays (montmorillonite, MMT) and TiO2 nanoparticles have also been successfully produced using the electrospinning technique. [23]

1.4 Composite materials

Implants must perform as the tissues for which they substitutes. Efforts to satisfy the latter criterion led to the investigation of structural biomaterial composites. A composite material consists of two or more physically and/or chemically distinct, suitably arranged or distributed materials with an interface separating them. It has characteristics that are not depicted by any of the components in isolation, these specific characteristics being the purpose of combining the materials. [20] The term "composite" is usually reserved for those materials in which the distinct phases are separated on a scale larger than the atomic, and in which properties such as the elastic modulus are significantly altered in comparison with those of a homogeneous material. Natural composites include bone, wood, dentin, cartilage, and skin. Natural foams include lung, cancellous bone, and wood. Natural composites often exhibit hierarchical structures in which particulate, porous, and fibrous structural features are seen on different micro-scales. Composite materials offer a variety of advantages in comparison with homogeneous materials. These include the ability for the scientist or engineer to exercise considerable control over material properties. There is the potential for stiff, strong, lightweight materials as well as for highly resilient and compliant materials. [21] The properties of composite materials depend very much upon structure. Composites differ from homogeneous materials in that considerable control can be exerted over the larger scale structure, and hence over the desired properties. In particular, the properties of a composite material depend upon the shape of the heterogeneities, upon the volume fraction occupied by them, and upon the interface among the constituents. The shape of the heterogeneities in a composite material is classified as follows. The factors that most contribute to the engineering performance of a composite include:

1. Materials that make up the individual components
2. Quantity, form, and arrangement of the components
3. Interaction between the components

Of these, the reinforcement system in a composite material strongly determines the properties achievable in a composite. It is thus convenient and common to classify composites according to the characteristics of the reinforcement. These can include the shape, size, orientation, composition, distribution, and manner of incorporation of the reinforcement. For the purposes of a discussion of biomedical composites, this results in two broad groups, namely, fiber-reinforced and particle reinforced composites. Figure 4

shows further divisions within these groups.

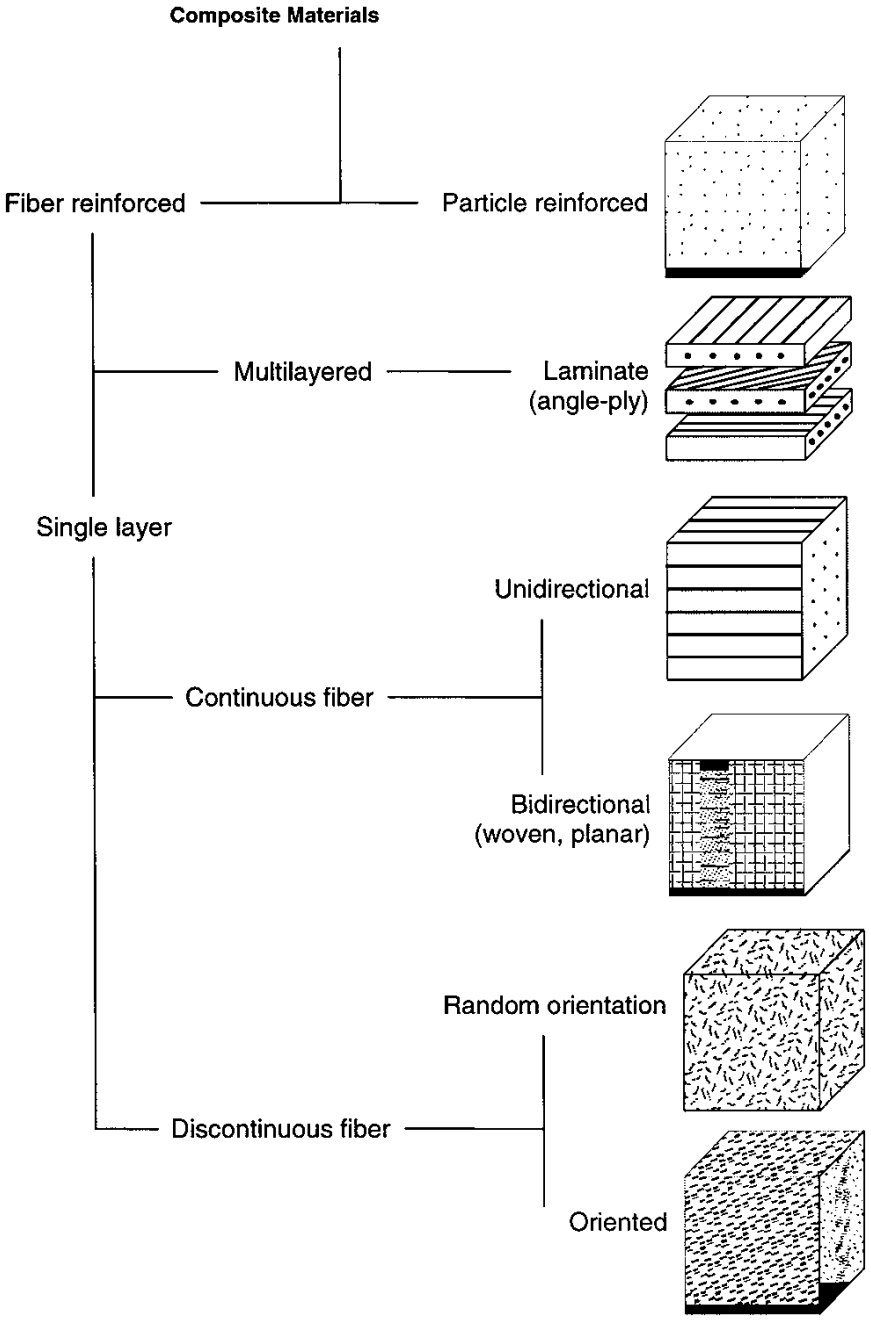

Figure 4 – Classification of biomedical composite materials. [20]

If one phase consists of voids, filled with air or liquid, the material is known as a cellular solid. If the cells are polygonal, the material is a honeycomb; if the cells are polyhedral, it is foam. It is necessary in the context of biomaterials to distinguish the above structural cells from biological cells, which occur only in living organisms. In each composite structure, we may moreover make the distinction between random orientation and preferred orientation.

Composite materials can also be broadly classified based simply on the matrix material used. This is often done more for processing than for performance purposes. Thus there are polymer-matrix composites (PMCs), ceramic-matrix composites (CMCs), or metal-matrix composites (MMCs). The last type is an advanced composite uncommon in biomedical applications and is mostly used for high-temperature applications.

The matrix in a composite is the continuous bulk phase that envelopes the reinforcement phase either completely or partially. It holds the fibers or particles in place, and in oriented composites, it maintains the preferred direction of fibers. The matrix transfers the applied load to the reinforcement and redistributes the stress. When used with brittle fibers, the matrix helps increase fracture toughness because it is typically of a lower stiffness material and can tolerate greater elongation and shear forces than the reinforcement. The matrix also determines the environmental durability of the composite by resisting chemical, hygroscopic, and thermal stresses and protecting the reinforcement from these stresses. Processing characteristics of a composite are also greatly influenced by the matrix. Common matrices in biomedical composites are listed in Table 1. In most medical applications thermoplastics are the matrix materials of choice due to their nonreactive nature, processing flexibility, generally greater toughness, and biodegradation possibility. New matrices are constantly being developed for medical applications that have designed reactivity, flexibility, and strength. Resorbable matrices are useful when a composite is not permanently needed once implanted, but it is challenging to design a stiff reinforcing material that has a comparable degradation rate to such matrices. Ceramic matrices are used for their compressive properties and bioactive possibilities but suffer from poor fracture toughness.

Fibers have a very high aspect ratio of length to diameter compared with particles and whiskers, and the smaller the diameter, the greater is the strength of the fiber due to a reduction in surface flaws. Fibers are often manufactured as continuous filaments, with diameters in the range of 5 to 50 μm, and then they are arranged to produce tows, yarns, strands, rovings, mats, etc. Whiskers are fibers made of single crystals with very small diameters around 10 μm, but their aspect ratio is high (>100). They have very high strengths but also high manufacturing cost. Compared with continuous-fiber composites, short-fiber composites are less efficient in the use of fibers and in achieving a desired orientation, but they are also less limited in design and processing possibilities and can come very close to achieving their theoretical strength.

Both continuous and short fibers can be oriented in one, two, or three dimensions, resulting in unidirectional, planar, and random reinforcement systems. The volume fraction of fibers oriented in a given direction strongly affects the physical properties of a composite in that direction. Unidirectional and planar reinforced composites exhibit anisotropy. Table 1 lists some fibers common in biomedical composites. There are many naturally occurring fibers, such as cotton, flax, collagen, jute, wood, hemp, hair, wool, silk, etc., but these have extremely varying properties and present many processing challenges. Among these, collagen fibers have been successfully utilized in tissue engineering of skin and ligament. Borosilicate glass fiber is ubiquitous in the composites industry but not common in biomedical composites, where, instead, adsorbable bioglass fibers made from calcium phosphate have found some applications. Carbon fiber is as strong as glass fiber but is several times stiffer owing to its fine structure of axially aligned graphite crystallites and is also lighter than glass. It is used extensively to make high-strength lightweight composites in prosthetic structural components, where the fatigue resistance of carbon-fiber composites is also an advantage.

Properties such as dimensional stability, electrical insulation, and thermal conductivity, can also be controlled effectively by particles, especially when added to polymer matrices. Particulate reinforcement is randomly distributed in a matrix, resulting in isotropic composites. Particles can either strengthen or weaken a matrix, depending on its shape, stiffness, and bonding strength with the matrix. Spherical particles are less effective than platelet or flakelike particles in adding stiffness. For these reason a different classification for inclusion shape categories can be: 1) particles, with no long dimension, 2) fibers, with one long dimension, and 3) platelets or laminas, with two long dimensions. Particulate inclusions may be spherical, ellipsoidal, polyhedral, or irregular.

Hard particles in a low-modulus polymer increase stiffness, whereas compliant particles such as silicone rubber, when added to a stiff polymer matrix, result in a softer composite. Fillers can be defined as nonreinforcing particles such as carbon black and glass microspheres added more for economic and not performance purposes, although they can affect composite properties. Particulate reinforcement in biomedical composites is used widely for ceramic matrices in dental and bone-analogue applications. The most common such particle form is hydroxyapatite, a natural component of bone where it exists in a composite structure with collagen.

Hydroxyapatite particles have very poor mechanical properties and may serve more as a bioactive than reinforcement component.

Table 1 – Constituents of Biomedical Composites. [20]

Matrix	Fibers	Particles
Thermosets	*Polymers*	*Inorganic*
Epoxy	Aromatic polyamides (aramids)	Glass
Polyacrylates	UHMWPE	Alumina
Polymethacrylates	Polyesters	*Organic*
Polyesters	Polyolefins	Polyacrylate
Silicones	PTFE	Polymethacrylate
Thermoplastics	*Resorbable polymers*	
Polyolefins (PP, PE)	Polylactide, and its copolymers with polyglycolide	
UHMWPE	Collagen	
Polycarbonate	Silk	
Polysulfones	*Inorganic*	
Poly(ether ketones)	Carbon	
Polyesters	Glass	
Inorganic	Hydroxyapatite	
Hydroxyapatite	Tricalcium phosphate	
Glass ceramics		
Calcium carbonate ceramics		
Calcium phosphate ceramics		
Carbon		
Steel		
Titanium		
Resorbable polymers		
Polylactide, polyglycolide and their copolymers		
Polydioxanone		
Poly(hydroxy butyrate)		
Alginate		
Chitosan		
Collagen		

The transfer and distribution of stresses from the matrix to the fibers or particles occur through the interface separating them. The area at the interface and the strength of the interfacial bond greatly affect the final composite properties and long-term property retention. A low interfacial area denotes poor wetting of the fiber with the matrix material. Wetting can be enhanced by processing methods in which there is greater pressure (metal matrices) or lower-viscosity flow (polymer matrices). When mechanical coupling is not sufficient, coupling agents are often used to coat fibers to improve chemical compatibility with the matrix. Interfacial shear strength determines the fiber-matrix debonding process and thus the sequence and relative magnitude of the different failure mechanisms in a composite. Strong interfaces common in polymer matrix composites make ductile matrices very stiff but also lower the fracture toughness. Weak interfaces in ceramic matrix composites make brittle matrices tough by promoting matrix crack but also lower strength and stiffness. [20]

1.5 PLA nanocomposites

Inorganic or organic nanoparticles have been incorporated to enhance the mechanical, barrier and thermal properties of PLA. Unlike micro- and macro-scaled particles (e.g., talc, glass fiber, carbon particles, etc.), nanoparticles can improve material properties at much lower added quantities (2–8 wt. %). Over the past few years, various nanomaterials have been investigated for reinforcing PLA, including layered silicates [24], carbon nanotube [25], hydroxyapatite [26], layered titanate [27], aluminum hydroxide [28], etc. Among the nanomaterials investigated, layered silicate clays have been studied in the greatest detail by researchers from both academia and industry. The heightened interest for these nanofillers can be attributed to their ability to dramatically improve material properties of the nanocomposite structures as compared with the pure PLA, including improved mechanical and flexural properties, elevated heat distortion temperature, enhanced barrier properties and accelerated biodegradation [24][29][30][31].

1.6 Graphene-based nanocomposites

Various polymers and nanoparticles (metal, metal oxide, semiconductor) composites have been developed based on the unique properties of graphene. Graphene possesses similar mechanical properties as CNTs but has superior electrical and thermal properties, and larger surface area (2620 m^2/g) because of its 2-dimensional crystal structure. The mechanical exfoliation of graphite is not suitable for large scale production, while chemical oxidation of graphite into graphite oxide offers an easy path to obtain graphene oxide in large quantity. This can then be reduced chemically, electrochemically or thermally into graphene. The bulk production of GO and RGO has given opportunities to explore this flat structure of carbon with polymer and nanoparticles in composites.

Graphene and its derivatives as fillers for polymer matrix composites have shown a great potential for various important applications. In the past few years, researches have made successful attempts for GO and graphene–polymer composites similar to CNT-based polymer composites. 2-D graphene has better electrical, thermal and mechanical properties as well as higher aspect ratio and larger surface area than other reinforced materials such as CNTs, fibers of carbon and Kevlar. Its reinforcement can offer

exceptional properties in composites and applications in the field of electronics, aerospace, automotive and green energy. The recent advancement in bulk synthesis processes of graphene and RGO has generated great interest to incorporate such unique material into various polymer matrices. Several challenges need to be overcome to realize graphene or graphene oxide based polymer composites,

1. Functionalization of graphene sheets
2. Homogeneous dispersion of materials with minimal restacking
3. Effective mixing of graphene oxide and graphene with polymer
4. Understanding of the interfacial structure and properties
5. Controlling the folding, crumpling and bending of graphene materials

Two potential approaches are commonly used to produce a single layer of graphene with high yield: (1) chemical and (2) thermal reduction of exfoliated sheets of graphene oxide, as explained in earlier sections. Both the methods disrupt the conjugated electrical structure of graphene and re- duce the electrical conductivity. On the other hand, the functional groups introduced by these invasive approaches can be used to achieve good dispersion of derived graphene in different solvents. Numerous efforts have been made to improve the dispersion of GO and RGO by functionalizing the use of organic molecules compatible with the polymer matrix to enhance interfacial interaction with matrix. For example, GO has carboxylic, hydroxyl and epoxy groups on the surface which improve its dispersion in water and keep individual layers separated from each other. However, these functional groups and defects on GO make it electrically insulating and thermally unstable, and the removal of these functional groups during reduction makes RGO hydrophobic and increases tendency to agglomerate irreversibly in an aqueous medium unless stabilized by polymers and surfactants. The dispersion behavior of GO in different organic solvents can guide the selection of compatible polymer matrix for bulk synthesis. The dispersion of graphene oxide and reduced graphene against their agglomeration in organic solvents, after complete exfoliation of graphitic layers, has been achieved by surface functionalization through non-covalent and covalent bonding. Various organic functional groups such as polystyrene [32], 1-pyrenebutyrate [33], dopamine [34], 7,7,8,8-tetracyanoquinodimethane [35], coronene carboxylate [36] have been used to produce stable aqueous and organic solvent dispersion and facilitated nanocomposite synthesis to induce desirable properties.

The method of solution blending, melt mixing, and in situ polymerization are the most

common synthesis strategies of the polymer matrix composites. Solution blending is the most common technique to fabricate polymer-based composites provided the polymer is readily soluble in common aqueous and organic solvents, such as water, acetone, DMF, chloroform, DCM and toluene. This technique involves the solubilization of the polymer in suitable solvents and mixing with the solution of the dispersed graphene suspension. The polar polymers including PMMA, PAA, PAN and polyesters have been successfully mixed with GO in solution blending where the GO surface was usually functionalized by isocyanates, alkylamine, alkyl-chlorosilanes, etc., to improve its dispensability in organic solvents. For instance, esterificated GO was mixed with PVA dissolved in DMSO to fabricate the PVA–GO nanocomposite. To homogenize the dispersion of graphene sheets, ultrasonic power can be used to produce metastable suspension. It is important to note that long time exposure to high power ultrasonication can induce defects in graphene sheets which are detrimental to the composite properties. Functionalization of graphene sheets may help in obtaining a higher loading of sheets and allow dispersion in water and other organic solvents. During the blending, the polymer coats the surface of the individual sheet and interconnects each sheet after the solvents are removed. Solution blending of GO and RGO sheets tend to agglomerate during slow solvent evaporation, resulting in inhomogeneous distribution of sheets in polymer matrix. The distribution can be controlled by controlling the evaporation time using spin coating or drop casting. Various polymer composites such as graphene–PVA, GO–PVA, graphene–PVC, PVA–GO layer by layer assembly, and PVDF-thermally reduced graphene have been prepared using this technique.

Melt mixing technique uses a high temperature and shear forces to disperse the reinforcement phase in the polymer matrix. The process avoids the use of toxic solvents. The high temperature liquefies the polymer phase and allows easy dispersion or intercalation of GO and reduced graphene sheets. The melt mixing is less effective in dispersing graphene sheets compared to solvent blending due to the higher viscosity of the composite at increased sheets loading. The process can be applicable to both polar and non-polar polymers. However, this technique is more practical for thermoplastic manufacturing composite in large scale. Varieties of graphene reinforced composites such as, exfoliated graphite–PMMA, graphene–polypropylene (PP), GO-poly (ethylene-2,6- naphthalate) (PEN) and graphene–polycarbonate, are prepared by this method. Low throughput of chemically reduced graphene restricts the use of graphene in the melt mixing process. However, graphene production in bulk quantity in thermal reduction

can be an appropriate choice for industrial scale production. The loss of the functional group in thermal reduction may be a hurdle in obtaining homogeneous dispersion in polymeric matrix melts especially in non-polar polymers. Kim and Macosko have not observed significant improvement in mechanical properties due to the elimination of the oxygen functional groups, which affected the interfacial bonding in graphene composite with polycarbonate and PEN, and the defects caused by high temperature reduction.

In situ polymerization starts with the dispersion of GO or RGO in monomer followed by the polymerization of the monomers. Like solution blending, functionalized graphene and GO sheets can improve the initial dispersion in the monomer liquid and subsequently in the composites. The in situ polymerization technique enables the covalent bonding between functionalized sheets and polymer matrix through various condensation reactions. On the other hand, non-covalent bonded composites such as PMMA–GO [37], PP–GO [38] and PE-graphite [39] have also been prepared by this technique. Extensive research has been performed on producing epoxy- based nano composites using in situ polymerization where sheets are first dispersed into resin followed by curing by adding hardener. Recently, graphene oxide sheets have been used for Mg/ Ti catalysis support for in situ Ziegler–Natta polymerization of PP [40]. The prepared composite showed a good exfoliation of GO and homogeneous dispersion in PP ma- trix, leading to high electrical conductivity. In situ polymerization has also been explored widely for the high level of dispersion of graphite-based layered structure in a polymer matrix, such as expanded graphite and graphite oxide. The in situ polymerization increases interlayer spacing and exfoliates the layered structure of graphite into graphite nano plates by the intercalation of monomers that generate polymers after polymerization, producing well-dispersed graphene in a polymer matrix. This approach has produced a variety of composites, such as PANI–GO/PANI–graphene, graphene nanosheet/carbon nanotube/polyaniline, and PANI–GO [41]. [23]

1.6.1 Composites characterization

After the synthesis of the biomaterial it is necessary to advance to the phase of physiochemical characterization of the composite. Some of the usual methods are:

Thermal Analysis gives range information about the parameters and characteristics of the material, like glass transition temperature, crystallinity, the presence of possible solvents, and the extent of cross linking reaction of the thermoplastic materials.

Knowledge of these properties is essential for both the selection of the type of processing or conditions of manufacturing. Also, complete physical characterization of the material, being necessary for defining its use.

Infrared Spectroscopy is used to identify molecules and the types of bonds inside the polymer structure. Chemical bonds give absorption bands whose frequently depends on the nature of the bonds, identifying molecular groups with characteristic absorption bands. The interpretation of an infrared spectrum is not as easy as it may seem. In fact, some bands can obscure others. Also, superposition of bands that shift because of structural characteristics can be mistaken for bands of a totally different group. Therefore, for exact interpretation, unshifted bands should be used to determine structural characteristics.

Scanning electron microscopy is an often used instrument for analyzing the morphological structure of materials, because of rapid and easy execution. SEM allows obtaining information about the structure and interaction between fiber and matrix composite. Also, yields information about the type of fracture, the deformation of materials, and the presence of micro voids in the system. Such information is fundamental for the optimum use of material.

Mechanical testing measures the ability of the material to resist a particular loading (tensile, compressive, bending). The response of the material is in terms of ultimate strength and deformation. Characteristic parameters that one extracts form stress-strain curves are: 1) elastic modulus: the slope of the linear part of the stress-strain curve. It is usually called Young´s modulus. 2) secant modulus: the relationship between force and deformation at any point along the stress-strain curve. 3) strain-at-break: the strain the material sustains immediately before rupture. 4) ultimate strength: the maximum force supported by the material. 5) rupture strength: the force the material supports immediately before rupture. Values of force and deformation at the yield point are of particular importance in the mechanical characterization of polymeric materials. The yield point can be defined as the value of stress where the material changes from prevalent elastic to plastic response. In plastic response, deformation becomes permanent and is no longer reversible on removal of the load. Materials are categorized in terms of their strength, strain-at-break, and elastic modulus. These parameters are tied to the physical properties of the material and processing conditions. The properties are molecular weight, degree of crystallinity, and amount of cross-linking.

Durability of a material is an important parameter for planning prosthesis. Fatigue gives an idea of durability under cyclic loading. Fatigue testing for biomedical applications is not well defined. It is very difficult to correlate fatigue results with *in vivo* performance. This is because there is still much unknown about interactions among cells, tissues, and the material. Yet, fatigue testing can indicate the performance of the material once implanted. [42]

1.6.2 Mechanical properties

The high mechanical performance (elastic modulus and tensile strength) of graphene sheets have attracted the attention of researchers. The polymer reinforced with graphene has been employed to explore intrinsic strength (125 GPa) and elastic modulus (1.1 TPa) of nanosheets to bulk polymer composites. Similar to other composites, the mechanical properties are dependent on the reinforcement phase concentration and distribution in the host matrix, interface bonding, and reinforcement phase aspect ratio, etc. Although the pristine graphene has the highest theoretical strength, the presence of functional groups on the GO surfaces has the additional benefits of its high level of dispersion in polar solvents and water. The improved GO/polymer interaction facilitates high molecular level dispersion and enhanced interfacial interaction, leading to high mechanical properties. The interaction of graphene and polymer at the interface of effective load transfer has been extensively investigated. The tailoring of mechanical properties by a covalent and non-covalent bond configuration between the matrix and sheets reinforcement can provide exceptional features. The responsible Van der Waals forces and hydrogen-bond interactions were reported for improved mechanical properties Research in graphene-based composites has been concentrated on improving the stiffness and the mechanical strength using graphene as filler. Other mechanical properties, fracture toughness, fatigue, and impact strength of the graphene reinforced composites is also being studied. It has also shown that the graphene filler suppressed the crack propagation in epoxy polymer matrix. The improvement in fracture and fatigue resistance is similar to CNT and nanoparticles reinforcement but only needs one to two orders of magnitude lower weight fraction of graphene nanofiller to achieve the same degree of reinforcement. The superior mechanical properties of composite made of graphene platelets over carbon nanotubes is related to their high specific surface area, enhancing nanofiller matrix adhesion/interlocking arising from their wrinkled (rough)

surface and 2-D flat geometry.

The reduced gas permeability of the graphene reinforced polymer has also been demonstrated. The permeability of the gases is the gas channeling through the polymer. Various studies showed that the dispersion of impenetrable graphite nanoplatelets, graphene and GO sheets of the high aspect ratio and surface area, into polymer matrices provide a tortuous path for the diffusing gas molecules, enhancing the gas barrier properties as compared to neat polymer.. Among three commonly used techniques for composite production, the solvent-based blending technique has shown more effective distribution of sheets in polymer matrices. The oxygen permeability study by Drzal group on graphite nanoplatelets reinforcement on widely used and important thermoplastic, polypropylene indicated 20% improvement in gas barrier property at 3 vol. % [43]. Whereas, higher oxygen permeability was observed for other additives of different shapes and aspect ratios such as carbon black, nanoclay, and PAN-based carbon fiber for similar amount of loading. [44]

1.6.3 Biocompatibility

It has been shown in studies with mice that GO is biocompatible [6] up to blood concentrations of 10 $mg \cdot kg^{-1}$ [7]; since only small amounts of graphene oxide are needed to achieve desired performances, graphene based materials might be used in biomedical technology. [8] GO and graphene had been reported as efficient drug carriers [12] [13]. PLA is also used for this purpose [14]; development of hybrid vehicles for drug targeting can take advantage of both materials properties and originate synergistic effects. [15] Also several graphene based biosensors are being developed [16], these sensors can be used, for example, to detect drug concentrations on target places. Recent studies show that graphene substrates promote adherence of human mesenchymal stromal cells and osteoblasts [17], which can lead to better performance on tissues recovery using scaffolds containing graphene and graphene oxide. Due to their great potential several approaches are under study for future applications of these nanomaterials in biomedical engineering and biotechnology. [18]

1.7 Research objectives

1. Incorporate GO and graphene nanoplatelets (GNP) in PLA.
2. Using the solvent casting method to produce thin films of PLA, PLA + GO and PLA + GNP with different degrees of nanofillers incorporation.
3. Characterize morphologic, mechanic, gas permeability and biocompatibility properties of the produced films.
4. Analyse obtained results and perspective potential applications of produced materials.
5. Delineate strategies to improve properties of produced materials.

CHAPTER 2

METHOD

In our work, GO and graphene nanoplatelets (GNP) were incorporated in PLA thin films using a solvent-casting method. Thin films were obtained and characterized. The goal was to improve mechanical and gas permeability properties of PLA films.

2.1 Materials

Poly(lactic acid) (PLA) 2002 D (4% d-lactide, 96% l-lactide content, molecular weight 121400 $g \cdot mol^{-1}$), was obtained from Natureworks (Minnetonka, USA).

Graphene nanoplatelets (GNP) grade M5 (average thickness of 6-8 nm, maximum length of 5 μm and superficial area between 120 and 150 $m^2 \cdot g^{-1}$), were purchased from XG Sciences (Lansing, USA). According to the manufacturer, GNP was prepared by exfoliation of sulfuric acid-based intercalated graphite by rapid microwave heating, followed by ultrasonic treatment. [18]

Graphene oxide (GO) was synthesized according to the modified Hummer´s method. 100 ml of H_2SO_4 were added to 3 g of graphite at room temperature and the solution was cooled at 0 ºC using an ice bath, followed by gradual addition of 14 g of $KMnO_4$. Then 300 ml of distilled water were added, followed by addition of H_2O_2 (to reduce $KMnO_4$ excess) until oxygen release stopped. The solid was filtered and washed with HCl (0.1 M) and water. After resting overnight, the resultant solution was decanted and the remaining product was centrifuged 4 times at 2000 rpm, during 5 minutes. The solid was recovered and dried at 110 ºC for 48 h. [45]

2.2 Preparation of GO/GNP - PLA nanocomposites

GO was dispersed in acetone using an ultrasonic bath (Bandelin Sonorex RK 512 H) during 5 hours and then added to a PLA/chloroform solution and again sonicated for 15 minutes. Concentrations of GO relative to PLA were between 0.2 and 0.8 wt. %. Thin films (25-65 μm) were made by spreading the GO/PLA dispersion on a PTFE coated plate using the doctor blade technique. Solvent was removed by: a) exposing the film to

room conditions during 7 days, and b) in a vacuum oven at 40 °C, during 10 days. Films dried according to the first procedure retained residual chloroform, which acts as a plasticizer, as discussed below. The second method insured efficient solvent removal. Film thickness was measured with a digital micrometer.

GNP were dispersed in chloroform using ultrasound sonication during 2 hours and then dispersed in a PLA/chloroform solution. Concentrations of GNP relative to PLA were between 0.2 and 1.0 wt. %. Thin films were prepared and dried according to same procedures as the GO/PLA nanocomposites.

2.3 Characterization

Raman spectra of powders (GO and GNP) and films (PLA, PLA + GO 0.4 wt. % and PLA + GNP 0.4 wt. %) were obtained under ambient conditions using a 514.5 nm line of an argon-ion laser, in a backscattering geometry. The scattered radiation was analyzed using a Jobin–Yvon T64000 spectrometer equipped with a CCD (Charge-coupled device) and a photon-counting detector.

An ultraviolet–visible spectrophotometer (Perkin Elmer – Lambda 750) was used to evaluate the light transmittance of the films.

Optical microscopy images were obtained with an Olympus IX51 inverted microscope.

For transmission electron microscopy (TEM) visualization, PLA and PLA + GO films were prepared by ultramicrotomy (Leica EM UC6 - cryogenic chamber EM FC6) with diamond knifes at -30 ºC, samples and chamber at -100 ºC. Films were embedded in epoxy resin and sections (thickness 80 nm) collected on a DMSO solution. Images were obtained using a Transmission electron microscope (Zeiss 902A 80 kV Germany) on ATAF (Advanced Tissue Analysis Facility).

The morphology of GO and GNP were observed using scanning electron microscopy (SEM) FEI Quanta 400FEG, with acceleration tension of 3 kV. The powders were obtained by solvent evaporation after dispersion in chloroform and were applied on conductive carbon strips before visualization. PLA films selected for SEM analysis were cut transversely with a steel blade and applied on carbon tape. The film samples were then coated by sputtering a conductive Au/Pa layer.

Tensile properties of the films (dimension 60 mm × 20 mm, thickness 25 - 65 μm) were measured using a Mecmesin Multitest-1d motorized test frame, at room temperature. Loadings were recorded with a Mecmesin BF 200 N digital dynamometer (maximum

load 200 N), at a strain rate of 50 mm·min^{-1}. To ensure data accuracy and repeatability, at least 5 measurements were carried out for each film.

Glass transition temperatures (T_g), melting temperatures (T_m) and melting enthalpies of samples were determined with a Setaram DSC 131 device equipped with liquid nitrogen cooling; sample amounts ranged from 8 to 10 mg. The thermograms were recorded between 0 ºC and 200 ºC, at a heating rate of 10 ºC·min^{-1}, under N_2 flow.

Permeability towards O_2 and N_2 on PLA films was determined using the time-lag method. The experimental setup was composed of two tanks, feed (≈1 L) and permeate (53.44 cm^3), connected to a permeation cell. The whole unit was inserted in a thermostatic cabinet. The permeation cell has two compartments, feed and permeate, separated by the membrane (effective area of 11.04 cm^2) supported on a sintered disk. Initially, both chambers are evacuated, and, at a given instant, the membrane is made in contact to the feed at a constant pressure (Druck, PMP 4010, 0-2 bar). The permeate flow rate is obtained from the derivative of the permeate pressure within a small pressure variation. The pressure was read using a higher precision pressure sensor (Druck PMP 4010, 0-350 mbar). A detained description of the experimental setup and method can be found elsewhere [47].

Mouse embryo fibroblasts 3T3 (ATCC CCL-164) were grown in DMEM complete medium, at 37.8 ºC, in a fully humidified air containing 5% CO_2 (IR auto Flow). The cells were fed every 2–3 days. When cells reached confluence, the culture medium was discarded and the cells were detached with 2 mL of 0.25% (w/v) trypsin-EDTA [1:250, from porcine pancreas (Sigma)] solution for 15 min at 37.8 ºC, and 6 mL of DMEM complete medium was added to inactivate the trypsin after cell detachment. The cells were then centrifuged (10 min, 1000 rpm) and resuspended in culture medium before use.

MTT (3-(4,5-Dimethylthiazol-2-yl)-2,5-diphenyltetrazolium bromide solution), with a concentration of 0.5 mg/mL in PBS, in an amount equal to 10% of the culture volume was added to each well. After 3 h of incubation at 37.8 ºC, the MTT solution was removed and the insoluble formazan crystals formed in the bottom of the wells were dissolved in with 400 µl of isopropanol and centrifuged 2 minutes at 2000 rpm. The absorbance was measured at 550 nm using a plate reader (SynergyHT, BioTek).

Proliferation of fibroblasts in the surface of the films was evaluated for PLA, PLA + GO 0.4 wt. % and PLA + GNP 0.4 wt. %. Negative control (polystyrene) was also used.

Samples (radius = 13 mm) were sterilized by 1 minute immersion in ethanol (70 % v/v) and washed in PBS by the same procedure. Then samples were placed on the bottom of the wells and again washed with PBS. After that, 500 μL of DMEM complete medium with 5 x 10^4 fibroblast cells density were added to each well and incubated during 3h at 37.8 ^{o}C to allow adhesion. After this period, films were transferred to new plates and 500 μL of DMEM complete medium were added to each well. MTT assays were performed at 24, 48 and 72h. [48]

CHAPTER 3

RESULTS AND DISCUSSION

3.1 Dispersion of GO/GNP in PLA matrix

3.1.1 Raman spectroscopy

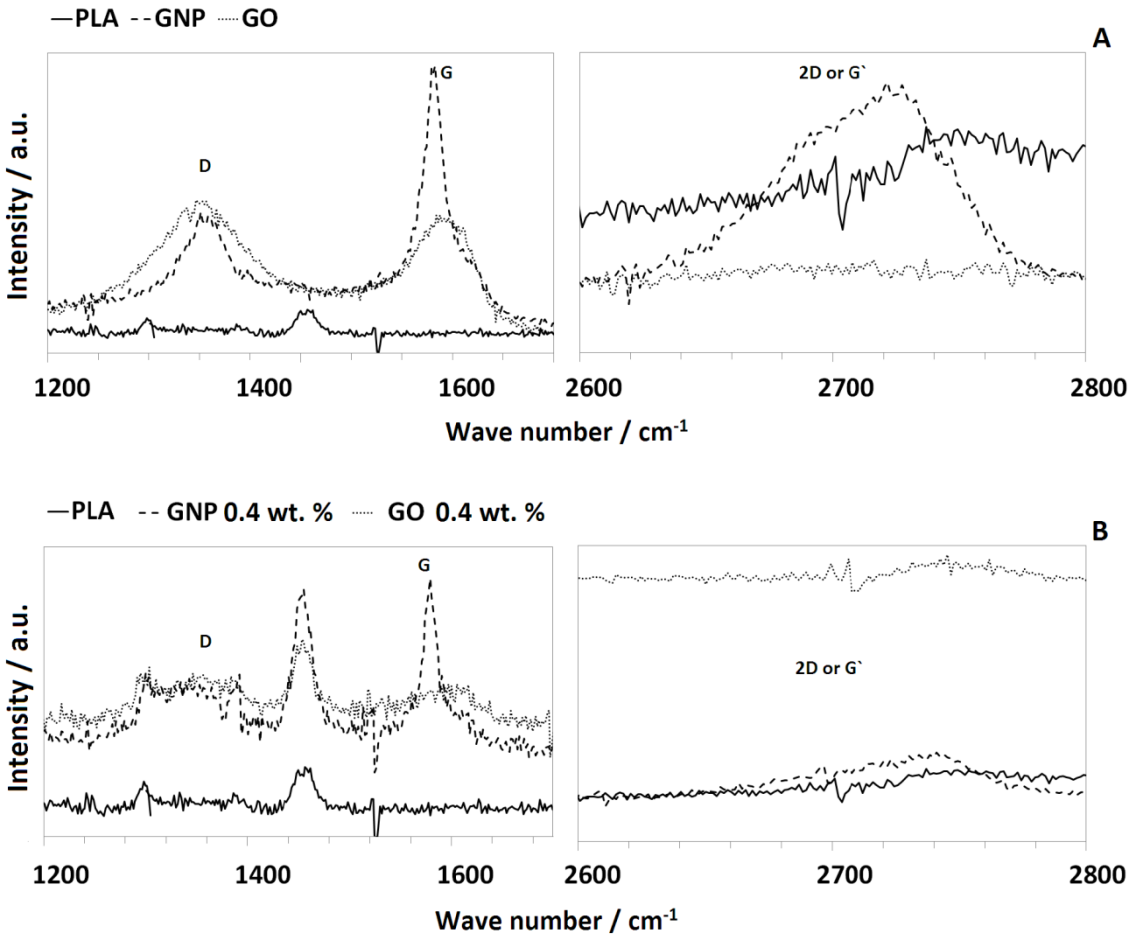

Figure 5 - Raman spectra of GO and GNP powders and pristine PLA film (A). Raman spectra of pristine PLA, PLA + GO 0.4 wt. % and PLA + GNP 0.4 wt. % films (B).

As seen in Figure 5.A, the Raman spectrum obtained for GNP is similar to the graphene spectrum. The ratio between D (1270-1450 cm^{-1}) and G (1580 cm^{-1}) bands is higher for

GO, due to electronic delocalization in sp^2 graphene structure caused by oxygen-containing functional groups. This also leads to weakening of π interactions between GO individual layers. Additionally, GNP presents an intense 2D or G` band, contrary to GO, indicating higher number of stacked graphene layers. [49] [50] PLA films exhibit characteristic bands at 1761, 1454 and 874 cm^{-1}. New bands appear in the spectra of PLA + GO and PLA + GNP (Fig. 5. B.) at wavelengths correspondent to GO and GNP spectra; this confirms the presence of the nanofillers in the PLA matrix. [51]

3.1.2 Optical and electronic microscopy

GO and GNP have distinct morphologies, which are visible in scanning electron microscopy of the respective powders. GO (Figure 6.A and B) consists of apparently well exfoliated oxidized graphene sheets, eventually forming agglomerates, maintaining the typical wrinkled appearance. GNP (6.C and D) are less exfoliated graphene platelets, formed by aggregation of 5 to 10 individual sheets, assuming more planar conformations. GNP particles are also larger than GO, as will become apparent in the composite film images shown next.

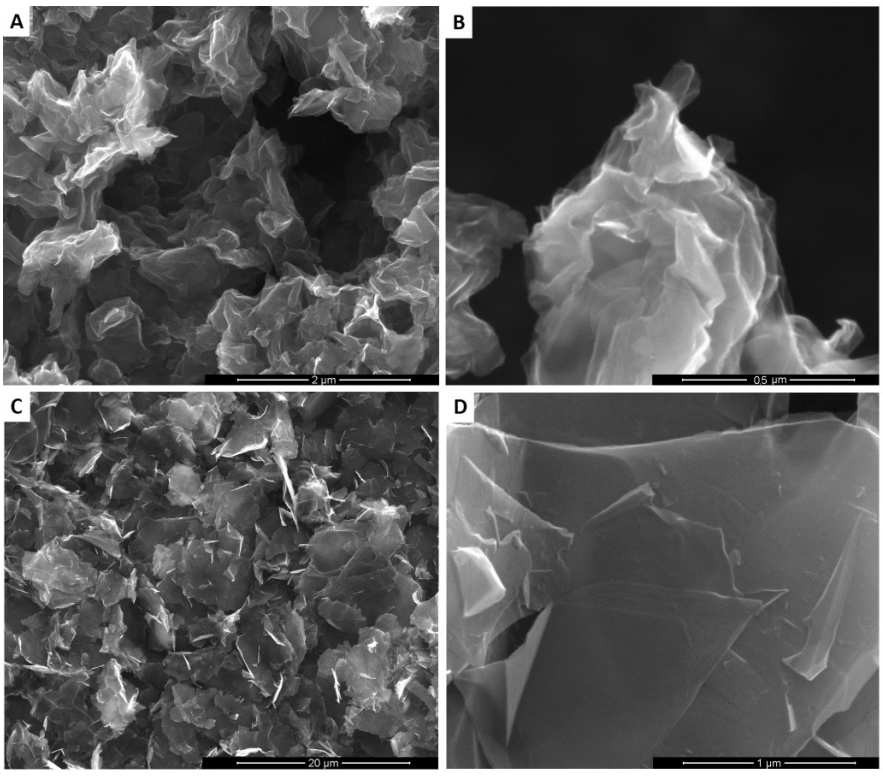

Figure 6 – SEM images of dry powders: A, B – GO (50000x, 200000x) and C, D – GNP (5000x, 100000x).

Because of the low thickness of the films, it is possible to qualitatively visualize the filler dispersion using optical microscopy. Figure 7 shows that, despite of the presence of some aggregates, both GO (Fig. 7. A) and GNP (Fig. 7. B) particles seem to be uniformly dispersed throughout the films. Due to small size, most GO sheets are hardly visible, except for the larger aggregates. GNP presents larger particles, as expected, some of which are superimposed. Images of unfilled PLA films, not shown here, revealed a clean, impurity free, interior.

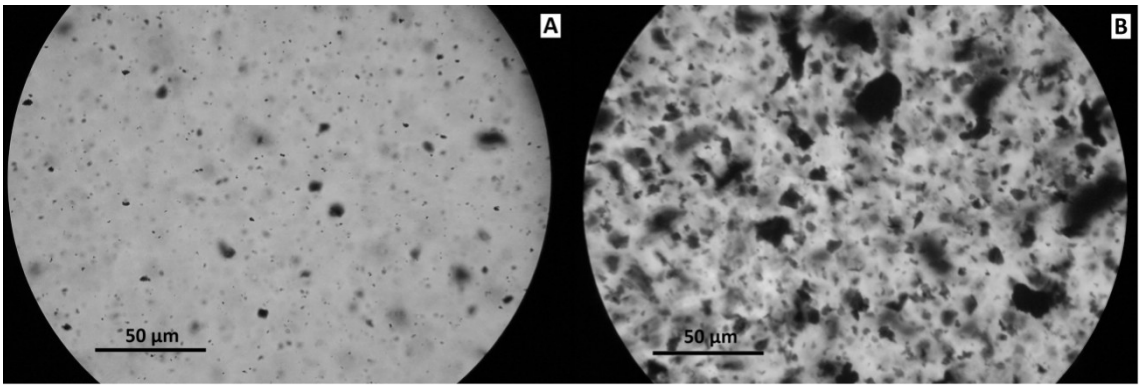

Figure 7 – Optical microscopy images of PLA films at 1000x magnification: A – PLA + GO 0.4 wt. %. B – PLA + GNP 0.4 wt. %.

Figure 8 shows a SEM image of a cut section of PLA film filled with GNP. Relatively large planar graphene platelets embedded in the polymer matrix can be seen, in accordance with the 5 µm maximum nominal length indicated by the manufacturer.

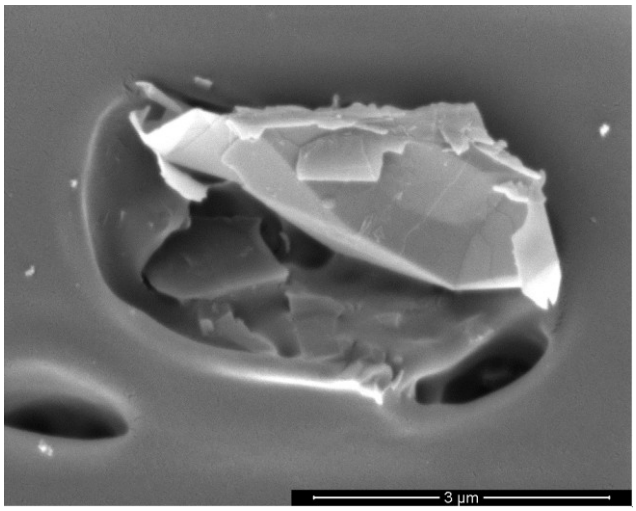

Figure 8 – SEM image of GNP after dispersion on PLA matrix (40000x).

Acceptable SEM images of GO particles in the PLA films could not be obtained due to sample instability when large magnifications are attempted. Useful information concerning the GO loaded films was therefore obtained by TEM imaging (Figure 9). Figure 9.B shows that GO is uniformly dispersed in the PLA matrix. GO single sheets (9.C) and some small aggregates (9.D) can be identified. The individual particle sizes are in the order of hundreds of nanometers.

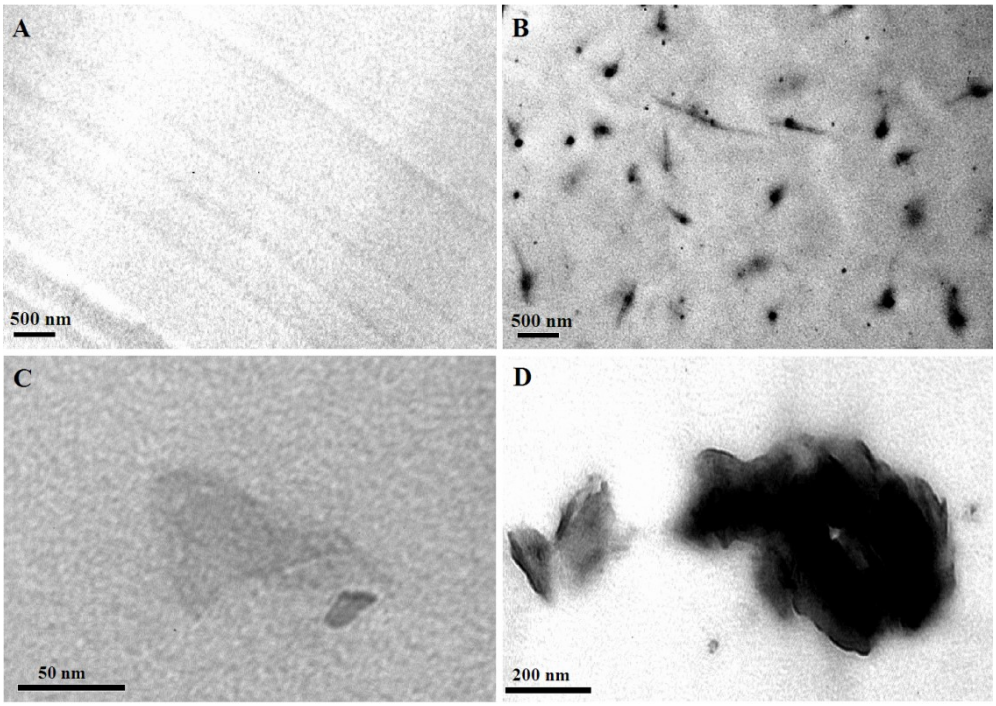

Figure 9 – TEM images of PLA and PLA + GO films. A - PLA (20000x). B, C, D - PLA + GO 0.4 wt. % (at magnifications 30000x, 250000x, 50000x, respectively).

Figure 10 shows photos of PLA films with different degrees of GO incorporation. It can be seen that transparency diminishes with the increase of nanofiller loading. This effect was even more pronounced when using GNP. Spectrophotometric transmission measurements of all films at 600 nm, shown in Table 1, confirm these observations. As expected, films filled with GO are more transparent than those containing equal loadings of GNP, due to disruption of the electronic conjugation within the graphene sheets in the oxidized state. [52] In all cases, the films were visually homogeneous.

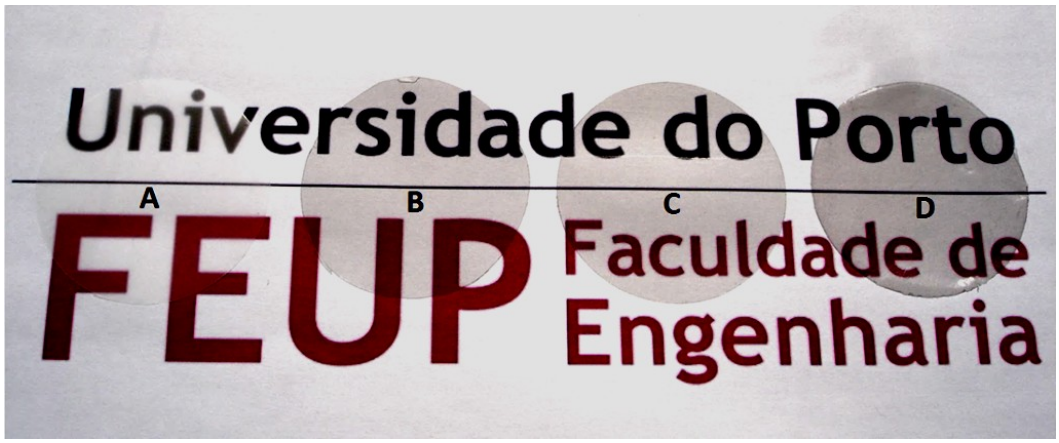

Figure 10 – Images of PLA and PLA + GO films. A - PLA, B - PLA + 0.2 wt. %, C - PLA + 0.4 wt. %, D - PLA + 0.6 wt. %.

Table 2 – Films transmittance at λ = 600 nm.

Samples	*% T*
PLA	92
GO 0.2 wt. %	81
GO 0.4 wt. %	76
GO 0.6 wt. %	72
GNP 0.2 wt. %	55
GNP 0.4 wt. %	24
GNP 0.6 wt. %	23

3.2 Mechanical properties

Mechanical properties of PLA, PLA + GO and PLA + GNP films were evaluated in traction tests. The films were dried in two different situations: at room conditions and in a vacuum oven at 40 ºC. In the first case, about 10 wt. % residual solvent is retained (determined by weighing), which acts as a PLA plasticizer, having a significant effect on mechanical performance. [53] The resulting stress-strain curves (Figure 11) show a well-defined yield point followed by some strain hardening. Since the films were applied by blade spreading, preliminary traction tests were performed in the direction of

spreading and in the perpendicular direction in order to check the existence of anisotropy. Identical results were obtained, therefore confirming that the films are mechanically isotropic.

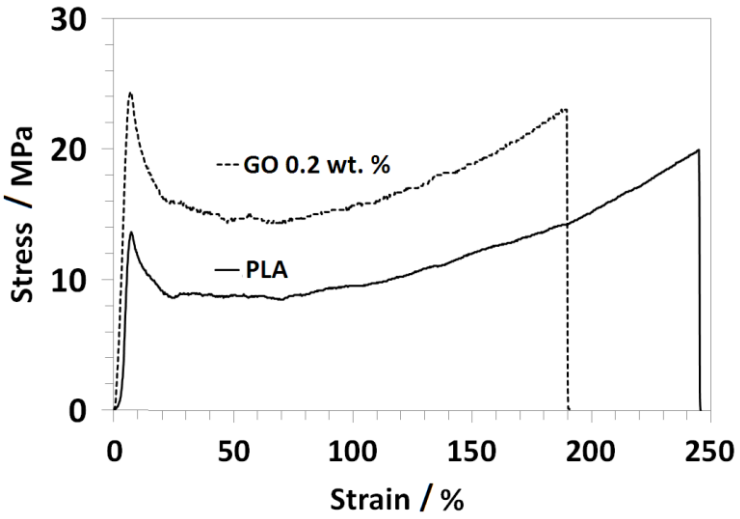

Figure 11 – Representative stress-strain curves for plasticized PLA and PLA + GO 0.2 wt. % films

For a GO content of 0.3 wt. %, the Young´s modulus increases by 115 % (Figure 12. A) and the yield strength by 95 % (Fig. 12. B), compared to pristine PLA films. For larger GO contents, the performance decreases, probably due to less homogeneous distribution and agglomeration of GO particles within the PLA matrix. The existence of an optimum loading can also be seen for a GNP content of 0.4 wt. %, for which Young´s modulus increases by 156 % (Fig. 12. A) and yield strength by 129 % (Fig. 12. B). The results are very similar for GO and GNP, the later seeming to yield slightly better results, but the differences are within the experimental error. The ultimate strength (Fig. 12. C), and the elongation at break measurements, did not show a defined dependence on the fillers content. This fact is not determinant, since for many applications only the properties at the yield point, and not at the fracture limit, are relevant for the performance of the material.

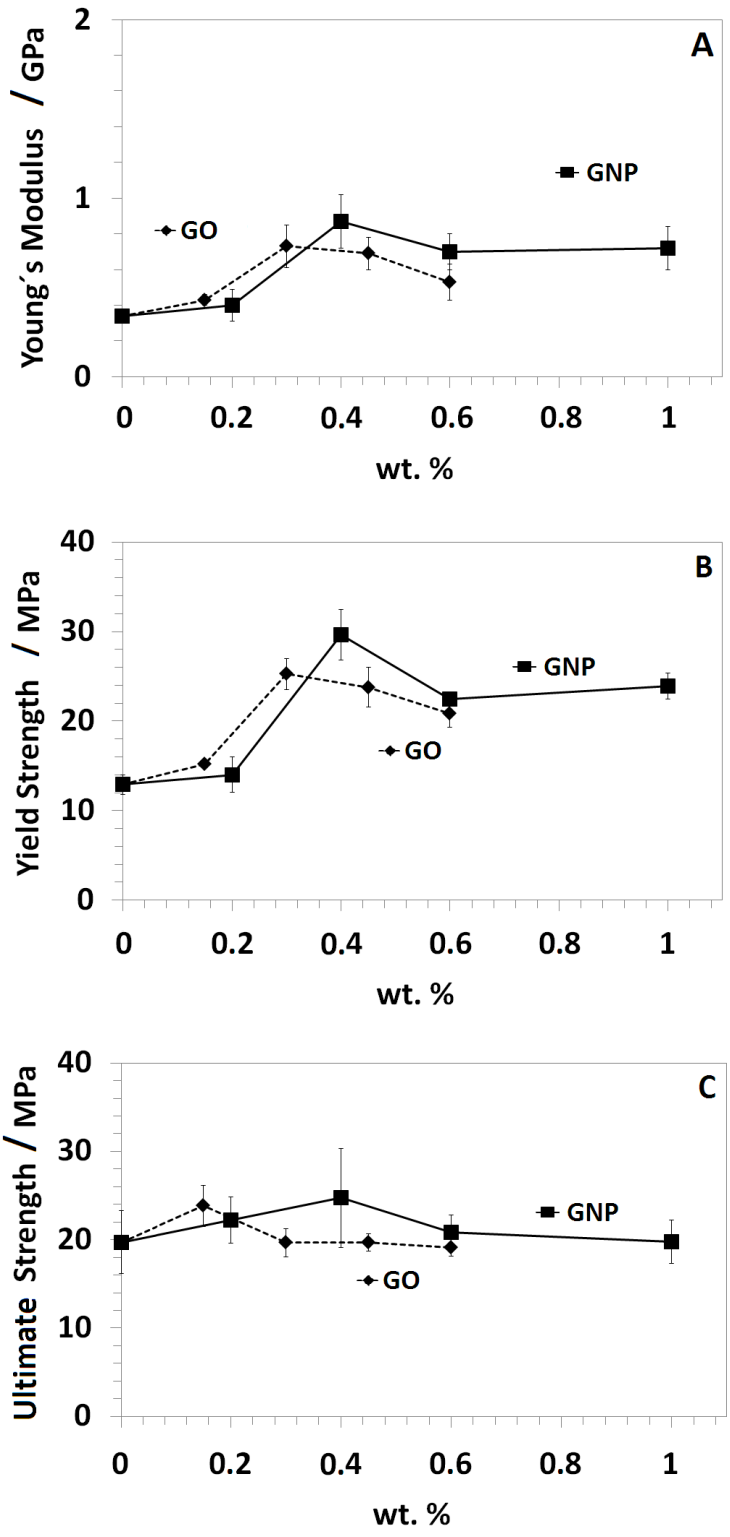

Figure 12 – Effect of increasing nanofiller load on mechanical properties of plasticized PLA films. Error bars represent the standard deviation computed from five measurements.

Films dried under vacuum are completely solvent free and are therefore not plasticized. These present stress-strain curves typical of a glassy polymer, as shown in Figure 13. Yielding behavior is not present, and elongation at break is significantly reduced: from values higher than 200 % to 3-4 %. These films also exhibit higher values of Young´s modulus (2-4 GPa) and tensile strength (about 50-60 MPa). Rhim and co-workers [54] had already reported the significant solvent-induced plasticization when solvent-cast PLA films are produced with incomplete drying.

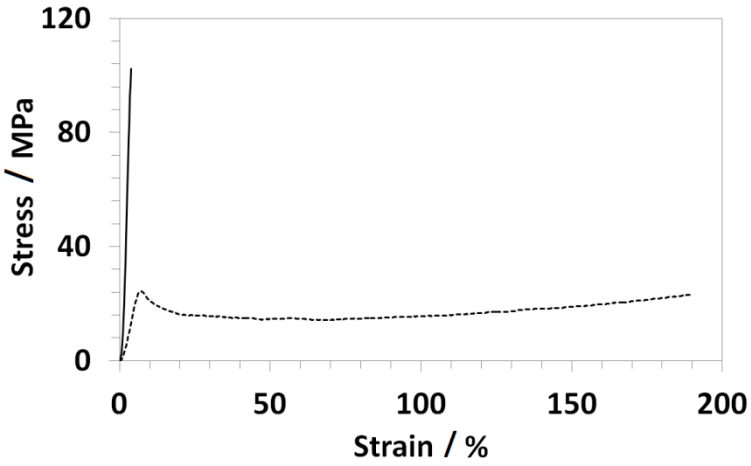

Figure 13 – Representative stress-strain curves for plasticized (dashed line) and unplasticized (solid line) PLA + GO 0.2 wt. % films.

The existence of an optimum loading can again be seen, as occurred with the plasticized material. Films with 0.4 wt % GNP content show an increase of 85 % in Young´s modulus (Fig. 14. A) and of 15 % in tensile strength (Fig. 14. B). Results for GO and GNP are again very similar. Nanofiller addition again did not have a significant effect on elongation at break (values not shown here).

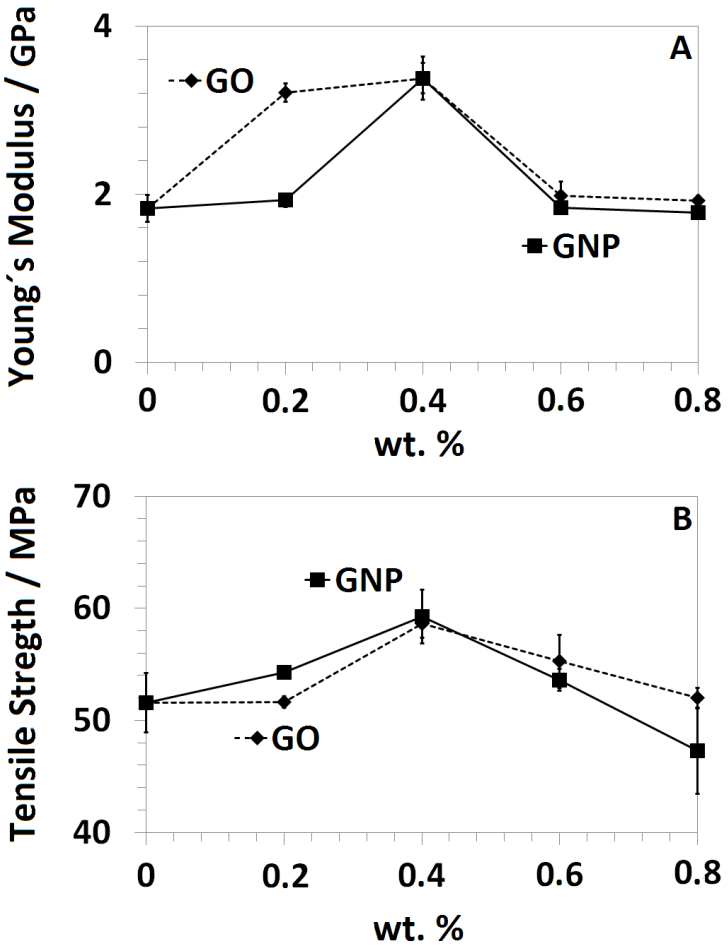

Figure 14 – Effect of increasing nanofiller wt. % on mechanical properties of PLA films after drying in a vacuum oven. Error bars represent the standard deviation computed from five measurements.

In principle, it would be expectable that incorporation of GO would lead to a stronger reinforcement effect than GNP, considering that the presence of oxidized groups in the whole surface would favor interactions with hydrophilic groups of PLA. [11] However, the wrinkled morphology of GO is less favorable than the planar geometry of GNP for interaction with the polymer matrix, which may explain the similarities in the results.

The results presented here show very significant improvements in mechanical properties with the addition of very small amounts of both GO and GNP. An optimum loading was identified for about 0.4 wt. %, indicating that for higher filler additions agglomeration effects overcome the reinforcement benefits. When solvent-plasticized PLA is used the range of improvement in mechanical performance by GO and GNP addition is larger. The significance of these results is more evident when comparing to other works reporting PLA reinforcement with carbon-based materials. Murariu and co-workers

[55], observed 30 % raise in Young´s modulus for incorporation of expanded graphite at 3 wt. % loading in PLA, on 3.1 mm thick test specimens. The results obtained by Wu and co-workers [56], showed improvements in tensile strength of about 20 % in PLA films after incorporation at 1-3 % loadings of chemically treated multi-walled carbon nanotubes (MWNTs) in an also chemically modified PLA matrix. Cao and co-workers [11] incorporated 0.2 wt. % of reduced GO in PLA, obtaining 18 % increase in Young´s modulus for 0.4-0.45 mm thick specimens.

3.3 DSC analysis

Differential scanning calorimetry analysis was performed for different filler loadings, on vacuum dried films. Figure 15, shows representative calorimetric curves obtained for PLA and PLA with 0.4 wt. % GO and GNP, after drying in a vacuum oven. In all curves the glass transition temperature (T_g) can be seen at around 50-60 ºC, immediately followed by a small hysteresis peak, associated to physical relaxation. Above 100 ºC, an excess crystallization endothermic peak is visible. Finally, melting takes place at about 150 ºC.

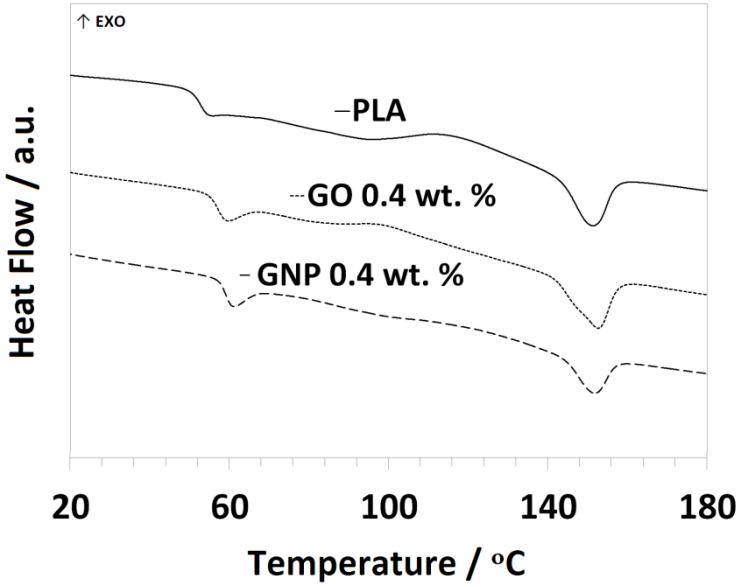

Figure 15 – Representative DSC curves for PLA films dried in vacuum oven.

Table 3 shows the values of T_g and T_m for all samples tested. Firstly, it must be noted that the T_g of unprocessed PLA is about 7 ºC higher than for solvent cast PLA. This is

due to formation of free volume within the polymer matrix when solvent is evaporated at 40 ºC. It is therefore noted that unprocessed PLA may present different properties from the films studied here, but this study concerns the effect of GO and GNP incorporation taking as reference solvent-cast PLA films.

As the films are loaded with nanofillers, T_g increases significantly in relation to the unloaded PLA films, denoting restricted molecular mobility associated with good filler-matrix interaction. A maximum is observed for 0.4 wt % loadings, coinciding with the optimum loading observed for mechanical properties. This effect is more pronounced with GNP (T_g is 2 ºC higher at same loading), probably due to the more planar geometry of the filler yielding more effective confinement of chain segment mobility. [57] Wu and Liao [55] also observed increases in T_g for incorporation of carbon nanotubes in PLA: a 4 ºC increase in T_g, but for higher loadings (3 wt. %). T_m shows no defined changes. A decrease in T_m would be observed if phase separation occurred, as reported in several works. [55][58]

Table 3 – Glass transition temperature and melting temperature results obtained for PLA films.

Samples	T_g °C	T_m °C
Unprocessed PLA	59.6	152.0
PLA	52.7	151.0
PLA + GO 0.2 wt. %	55.5	151.8
PLA + GO 0.4 wt. %	57.1	152.5
PLA + GO 0.6 wt. %	55.8	150.1
PLA + GNP 0.2 wt. %	58.5	150.1
PLA + GNP 0.4 wt. %	59.0	151.5
PLA + GNP 0.6 wt. %	58.0	150.9

3.4 Gas permeability properties

Permeability of the films towards oxygen and nitrogen was measured using the so-called time-lag method. Results are shown in Table 4. PLA permeability towards oxygen and nitrogen was close to the previously reported by Komatsuka and co-workers [39], although permeability can vary depending on PLA type and on membrane manufacturing process. The largest decreases in permeability were obtained for 0.4 wt. % of GO and GNP, corresponding to about a threefold decrease in permeability towards oxygen and a fourfold decrease towards nitrogen. For comparison, a twofold decrease in oxygen permeability was reported by Chang and co-workers [59] for the incorporation of 10 wt. % of various organic nanoclays in PLA films.

Table 4 – Effect of nanofillers incorporation on permeability of the PLA films towards O_2 and N_2.

Samples	O_2 $m^3 \cdot m \cdot m^{-2} \cdot s^{-1} \cdot Pa^{-1}$ x 10^{-18}	N_2 $m^3 \cdot m \cdot m^{-2} \cdot s^{-1} \cdot Pa^{-1}$ x 10^{-18}
PLA	3.76	1.10
GO 0.2 wt. %	1.34	0.271
GO 0.4 wt. %	1.23	0.306
GO 0.6 wt. %	1.49	0.502
GNP 0.2 wt. %	1.34	0.270
GNP 0.4 wt. %	1.20	0.250
GNP 0.6 wt. %	1.30	0.237

This gas permeability reduction is associated to a barrier effect created by the nanofillers. It could be expected that GNP, having a more planar configuration, would be more efficient in creating a tortuous path for permeation than the GO particles. That was not observed, and both fillers showed similar effects. This may be related to an absence of orientation of the GNP platelets along the film plane, which does not contribute for increasing tortuosity in the direction perpendicular to the film plane. A different manufacture method, e.g. extrusion, may have induced an effective difference in the permeation of GNP and GO.

3.5 Cell proliferation assay

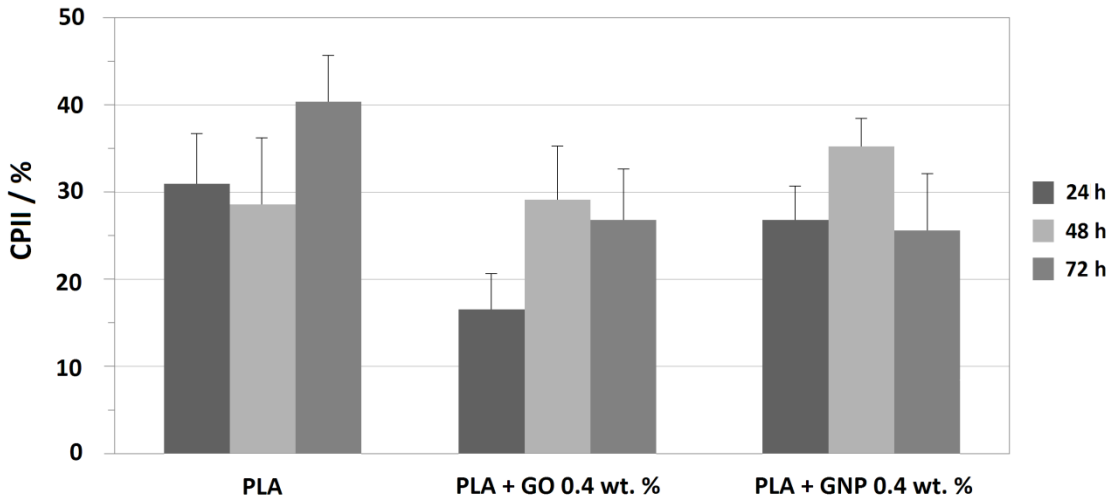

Figure 15 - Cell Proliferation Inhibition Index of Mouse Embryo Fibroblasts, Cultured on PLA, PLA + GO 0.4 wt. % and PLA + GNO 0.4 wt. %.

Figure 15, shows that cell proliferation inhibition index of mouse embryo fibroblasts, appear to be similar for cells grown on PLA and PLA with GO and GNP 0.4 wt. % incorporations films, until 72 h growth. Results indicate that GO and GNP presence inside the polymer, at low concentrations like these, doesn´t affect cellular proliferation at polymer/cells interface. This is in agreement with results obtained from Chang and co-workers [60], reporting that graphene oxide doesn´t have any effect on cells at low concentrations. Zhang and co-workers [61], also observed that no pathological changes were observed in examined organs when mice were exposed to 1 mg kg^{-1} body weight of GO for 14 days.

CHAPTER 4

CONCLUSIONS AND FUTURE WORK

The results presented here show that incorporation of very small loadings of GO or GNP (0.2 to 0.6 %) in PLA films significantly improves mechanical properties and reduces gas permeability towards oxygen. This confirms the reported potential of graphene-related materials in providing relevant performance gains at low loadings, thanks to the high specific area available for interaction with the polymer matrix. An optimum loading was identified for mechanical performance, corresponding to about 0.4 wt. % for both materials. This indicates that filler agglomeration may become a determinant effect at higher loadings.

The range of improvement in mechanical properties is more pronounced when plasticized PLA was tested. This opens interesting possibilities for tailoring mechanical performance of plasticized PLA, after the choice of an appropriate plasticizer.

This enhancement in mechanical properties may have impact in biomedical applications (*e.g.* sutures, scaffolds, implants, pharmaceutical packaging). In addition, oxygen permeation is reduced by the addition of the graphene-based fillers, which is paramount for food and medicine preservation, and, in the particular case of GO, film transparency is not significantly hindered. Packaging applications may therefore be explored.

It is coincidental that the two nanofillers tested (GO and GNP), being distinct in terms of morphology and surface chemical composition, yielded not very different results, both in mechanical and gas permeation tests. In the case of GO, optimizing the surface oxidation level may lead to improvement of the measured properties. Partial reduction of graphene oxide should yield more flat sheets (less inter-particle interaction) and increase contact area with the polymer. These aspects will be the subject of future work. Use of a different manufacture process, like film-extrusion, may additionally induce orientation of planar particles parallel to the film surface, maximizing the gas permeation barrier effect.

Results obtained for cellular growth on films, indicate that the incorporation of GO and GNP on PLA at low loadings, doesn´t affect cell proliferation at the surface of the polymer. This makes GNP and GO incorporation at low loadings in biomedical devices feasible, as well as their applications as drug carriers or biosensors.

REFERENCES

1. Armentano I and Kennya JM, *Polymer Degradation and Stability* **95**: 2126-46 (2010).

2. Drumright RE and Henton DE, *Adv. Mater* **12**: 1841-5 (2000).

3. Cabedo L and Giménez E, *Macromol. Symp* **233**: 191-7 (2006).

4. Kim K and Macosko W, *Macromolecules* **43**: 6515-30 (2010).

5. Dreyer DR and Ruoff RS, *Chemical Society Reviews* **39**: 228-40 (2010).

6. Chang Y and Wang H, *Toxicology Letters* **200**: 201-10 (2010).

7. Zhang X and Huang Q, *Carbon* **49**: 986–95 (2011).

8. Zhang L and Zhang Z, *Small* **6**: 537–44 (2010).

9. Pan Y and Li L, *Carbohydrate Polymers* **83**: 1908-15 (2011).

10. Song P and Fu S, *Polymer* **52**: 4001-10 (2011).

11. Cao Y and Wu P, *Carbon* **48**: 3834-39 (2010).

12. Zhang L and Zhang Z, *Small* **6**: 537-44 (2010).

13. Yang K and Liu Z, *Nano Lett.* **10**: 3318–23 (2010).

14. Kumari A and Yadav S, *Colloids and Surfaces B: Biointerfaces* **75**: 1–18 (2010).

15. Bai H and Shi G, *Advanced Materials* **23**: 1089-115 (2011).

16. Pumera M, *Chem Rec.* **9**: 211-23 (2009).

17. Kalbacova M and Kalbac M, *Carbon* **48**: 4323-29 (2011).

18. Wang Y and Lin Y, *Tends in Biotechnology* **29**: 205-12 (2011).

19. Ramakrishna S and Leong K, *Composites Science and Technology* **61**: 1189-224 (2001).

20. Arif Iftekhar, Biomedical Composites, in *Biomedical Engineering and Design Handbook: Applications*, ed by Kutz M, McGraw-Hill, New York, pp 339-45 (2009).

21. Chu CC, Biodegradable Polymeric Biomaterials: An Updated Overview, in *The Biomedical Engineering HandBook*, ed by Joseph D, CRC Press, Boca Raton, pp 719-25 (2000).

22. Nair L and Laurencin C, *Prog Mater Sci* **32**: 762–98 (2007).

23. Lim L and Rubino M, *Prog Mater Sci* **33**: 820–52 (2008).

24. Ray SS and Bousmina M, *Prog Mater Sci* **50**: 962–1079 (2005).

25. Chen G-X and Yoon J-S, *J Phys Chem B* **109**: 22237–43 (2005).

26. Kim H-W and Knowles JC, *J Biomed Mater Res A* **79**: 643–9 (2006).

27. Hiroi R and Ray SS, Shiroi T, *Macromol Rapid Commun* **25**: 1359–64 (2005).

28. Nishida H and Endo T, *Ind Eng Chem Res* **44**: 1433–7 (2005).
29. Yu L,and Li L, Polymer blends and composites from renewable resources. *Prog Polym Sci* **31**: 576–602 (2006).
30. Singh S and Ray SS, *J Nanosci Nanotechnol* **7**: 2596–615 (2007).
31. Pandey JK and Singh RP, An overview on the degradability of polymer nanocomposites. *Polym Degrad Stab* **88**: 234–50 (2005).
32. Wang G and Park J, *Carbon* **47**: 1359-64 (2009).
33. Xu YX and Shi GQ, *J Am Chem Soc* **130**: 5856-7 (2008).
34. C Xu LQ, Yang WJ and Fu GD, *Macromolecules* **43**: 8336-9 (2010).
35. Hao R and Hou Y, *Chem Commun* **48**: 6576-8 (2008).
36. Ghosh A and Rao CNR, *Chem Eur J* **16**: 2700-4 (2010).
37. Kalaitzidou K and Drzal LT, *Compos Sci Technol* **67**: 2045-51 (2007).
38. Kim H and Macosko CW, *Macromolecules* **41**: 3317-27 (2008).
39. Kim H and Macosko CW, *Polymer* **50**: 3797-809 (2009).
40. Huang Y and Dong J-Y, *Chem Mater* **22**: 4096-101 (2010).
41. Yan J and Shen XD, *J Power Sour* **195**: 3041-45 (2010).42. Ambrosio L, Peluso G and Davis PA, Biomaterials and their biocompatibilities, in *Human Biomaterials Applications*, ed by Wise DL, Humana Press Inc, New Jersey, pp 5-7 (1996).
43. Jiang X and Drzal LT, *Polym Compos* **31**: 1091-98 (2009).
44. Singh V and Seal S, *Progress in Materials Science* **56**: 1178–271 (2011).
45. Kalaitzidou K and Drzal LT, *Composites: Part A* **38**: 1675–82 (2007).
46. Tanaka D and Mendes A, Composite Graphene-Metal Oxide Platelet Method of Preparation and Applications. International Patent PCT/IB2010/055598 (2010).
47. Tomé L and Mendes A, *Carbohydrate Polymers* **83**: 836–42 (2010).
48. Carvalho J and Gama FM, *Journal of biomedical materials research. Part A* **93**: 389-99 (2010).
49. Ok Y and Nae-Eung L, *Composites: Part A* **in press** (2011).
50. Virendra S and Sudipta S, *Progress in Materials Science* **56**: 1178–271 (2011).
51. Qiang L and Chuanbao C, *Composites Science and Technology* **67**: 3023-30 (2007).
52. Bai H and Shi G, *Adv. Mater* **23**: 1089-115 (2011).
53. Rhim JW and Perry KW, *Journal of Applied Polymer Science* **101**: 3736-42 (2006).
54. Murariu M and Dubois P, *Polymer Degradation and Stability* **95**: 889-900 (2010).
55. Wu C and Liao H, *Polymer* **48**: 4449-58 (2007).
56. Miltner H and Mele B, *Polymer* **47**: 826-35 (2006).

57. Murariu M and Dubois P, *Polymer Degradation and Stability* **95**: 374-81 (2010).
58. Komatsuka T and Nagai K, *Desalination* **234**: 212–20 (2008).
59. Chang J and Sur GS, *Journal of Polymer Science: Part B* **41**: 94–103 (2003).
60. Chang Y and Wang H, *Toxicology Letters* **200**: 201-210 (2010).
61. Zhang X and Huang Q, *Carbon* **49**: 986–95 (2011).